
Since January 2020 Elsevier has created a COVID-19 resource centre with free information in English and Mandarin on the novel coronavirus COVID-19. The COVID-19 resource centre is hosted on Elsevier Connect, the company's public news and information website.

Biochemical Pharmacology 82 (2011) 1234–1249

Contents lists available at ScienceDirect

Biochemical Pharmacology

journal homepage: www.elsevier.com/locate/biochempharm

# Amiodarone impairs trafficking through late endosomes inducing a Niemann-Pick C-like phenotype

Elena Piccoli [a,1], Matteo Nadai [a,1], Carla Mucignat Caretta [b], Valeria Bergonzini [a], Claudia Del Vecchio [a], Huy Riem Ha [c], Laurent Bigler [d], Daniele Dal Zoppo [e], Elisabetta Faggin [f], Andrea Pettenazzo [g], Rocco Orlando [h], Cristiano Salata [a], Arianna Calistri [a], Giorgio Palù [a], Aldo Baritussio [h,*]

[a] Department of Histology, Microbiology and Medical Biotechnologies, University of Padova, via A. Gabelli 63, 35121, Italy
[b] Department of Human Anatomy and Physiology, University of Padova, via F. Marzolo 3, 35131, Italy
[c] Cardiovascular Therapy Research Laboratory, Clinical Research Center, University Hospital, Rämistrasse 100, 8091 Zürich, Switzerland
[d] Institute of Organic Chemistry, University of Zürich, Winterthurerstrasse 190, 8057 Zürich, Switzerland
[e] Department of Pharmaceutical Sciences, University of Padova, via F. Marzolo 5, 35131, Italy
[f] Department of Clinical and Experimental Medicine, University of Padova, via Giustiniani 2, 35128, Italy
[g] Department of Pediatrics, University of Padova, via Giustiniani 3, 35128, Italy
[h] Department of Medical and Surgical Sciences, University of Padova, via Giustiniani 2, 35128 Padova, Italy

ARTICLE INFO

*Article history:*
Received 5 May 2011
Accepted 20 July 2011
Available online 23 August 2011

*Keywords:*
Amiodarone
Dronedarone
Late endosomes
Niemann-Pick C
Phospholipidosis

ABSTRACT

Patients treated with amiodarone accumulate lysobisphosphatidic acid (LBPA), also known as bis(monoacylglycero)phosphate, in airway secretions and develop in different tissues vacuoles and inclusion bodies thought to originate from endosomes. To clarify the origin of these changes, we studied *in vitro* the effects of amiodarone on endosomal activities like transferrin recycling, Shiga toxin processing, ESCRT-dependent lentivirus budding, fluid phase endocytosis, proteolysis and exosome secretion. Furthermore, since the accumulation of LBPA might point to a broader disturbance in lipid homeostasis, we studied the effect of amiodarone on the distribution of LBPA, unesterified cholesterol, sphingomyelin and glycosphyngolipids. Amiodarone analogues were also studied, including the recently developed derivative dronedarone. We found that amiodarone does not affect early endosomal activities, like transferrin recycling, Shiga toxin processing and lentivirus budding. Amiodarone, instead, interferes with late compartments of the endocytic pathway, blocking the progression of fluid phase endocytosis and causing fusion of organelles, collapse of lumenal structures, accumulation of undegraded substrates and amassing of different types of lipids. Not all late endocytic compartments are affected, since exosome secretion is spared. These changes recall the Niemann-Pick type-C phenotype (NPC), but originate by a different mechanism, since, differently from NPC, they are not alleviated by cholesterol removal. Studies with analogues indicate that basic pKa and high water-solubility at acidic pH are crucial requirements for the interference with late endosomes/lysosomes and that, in this respect, dronedarone is at least as potent as amiodarone. These findings may have relevance in fields unrelated to rhythm control.


## 1. Introduction

Amiodarone is a cationic antiarrhythmic drug extensively used for the control of supraventricular and ventricular arrhythmias. Its action mechanism includes blockade of K- and Na channels and interference with β-adrenoreceptors and Ca currents [1,2]. Amiodarone has a large volume of distribution (66 l/kg), steady state serum levels between 0.7 and 3.7 μM, an elimination half-life of several weeks and a propension to accumulate in different tissues, like adipose tissue, skeletal muscle and the liver, but not in the brain [3–5]. Recent evidence suggests that accumulation in tissues might happen by at least two mechanisms, that is the association with cell membranes, due to the high lypophilicity of amiodarone, and trapping in the lumen of acidic organelles after protonation of the amine function present in the lateral group diethylamino-β-ethoxy [6,7]. Amiodarone catabolism includes stepwise dealkylation and deamination of the lateral group diethylamino-ethoxy, major metabolite being N-desethylamiodarone (MDEA) whose activity and serum levels are similar to those of

*Abbreviations:* LBPA, lysobisphosphatidic acid; ESCRT, endosomal sorting complex required for transport; VLP, virus like particles.

* Corresponding author. Tel.: +39 49 8212149; fax: +39 49 8212149.
*E-mail address:* aldo.baritussio@unipd.it (A. Baritussio).

[1] These authors contributed equally to this work.

0006-2952/$ – see front matter © 2011 Elsevier Inc. All rights reserved.
doi:10.1016/j.bcp.2011.07.090

the parent drug [8]. Chronic exposure to amiodarone induces the formation of vacuoles and inclusion bodies in blood leukocytes, cells of the corneal epithelium, skin cells, alveolar macrophages, liver cells and cardiomyocytes [7]. Although there is agreement that these structures derive from interference of amiodarone with the endocytic pathway, there is uncertainty about the set of endocytic organelles involved, the mechanism of formation of vacuoles and the origin of materials, both amorphous and membrane-like, accumulating in the lumen of inclusion bodies.

Regarding the section of the endocytic pathway involved, it has been claimed that amiodarone does not interfere with early compartments of the endocytic pathway, since the drug does not modify the distribution of the early endosomal marker EEA1 [6]. However this issue remains undecided, since some found no interference of amiodarone with the activity of diphtheria toxin, whose active moiety enters the cytoplasm from early endosomes [9], while others found that amiodarone inhibits the toxin [10]. On the other side several lines of evidence suggest that amiodarone interferes with late compartments of the endocytic pathway. In fact, (i) vacuoles and inclusion bodies bear the markers of late endosomes/lysosomes, like Rab7 and CD63 [6,7], (ii) patients treated with amiodarone accumulate in the airways lysobisphosphatidic acid (LBPA), also known as bis(monoacylglycero)phosphate [11], which is a component of late endosome lumenal membranes [12], (iii) amiodarone inhibits *in vitro* the activity of the anthrax toxin, whose subunits (edema factor and lethal factor) enter the cytoplasm from late endosomes/multivesicular bodies [10,13]. Thus far it is unknown whether amiodarone interferes with recycling endosomes or with the pathway connecting directly early endosomes with the Golgi. Nor is it known if amiodarone interferes with the ESCRT complex, a highly conserved set of proteins associated with a specialized portion of the early endosomes, necessary for the formation of lumenal vesicles and the eventual maturation of this compartment into multivesicular bodies [14]. The ESCRT system is also involved in membrane deformations topologically equivalent to endovesiculation, like cytokinesis and the budding of membrane bound viruses [14]. Interestingly mutations of the ESCRT system lead to phenotypes characterized by the presence of vacuoles and inclusion bodies bearing markers of both early and late endosomes [14].

The observation that patients treated with amiodarone accumulate LBPA, which is only detected in late endosomes and is intimately connected with unesterified cholesterol [12,15], suggests that the drug might alter the distribution of other lipids too, as found in Niemann-Pick type C disease, where mutations of NPC1 or NPC2 proteins cause the accumulation of free cholesterol, glycosphyngolipids, sphingosine, LBPA and sphingomyelin in late endosomes/lysosomes [16–20]. Interestingly in Niemann-Pick type C cells accumulating lipids not only are a manifestation of disturbed traffic, but also play a pathogenetic role, since alleviation of the phenotype can be obtained by decreasing cholesterol levels [21], by inhibiting glycosphingolipid synthesis [22] or by increasing lipid degradation [23]. Very recently it has been shown that Niemann-Pick type C cells try to combat cholesterol accumulation by increasing the secretion of exosomes[24], which are vesicles located in the lumen of late endosomes/multivesicular bodies destined to be secreted rather than to be destroyed [25]. We speculated that, as it happens in Niemann-Pick type C disease, increased LBPA levels observed in patients treated with amiodarone might point to a more complex disturbance in the homeostasis of cell lipids.

In order to clarify some of these issues, we examined the effects of amiodarone on different endosomal activities. These included transferrin recycling, ESCRT functionality (by evaluation of lentiviruses budding) and the pathway connecting early endosomes with the Golgi complex probed with Shiga toxin 1, which after processing within early endosomes, moves to the Golgi through vesicular intermediates [26]. Furthermore we analyzed the effect of amiodarone on the secretion of exosomes and on the distribution of lipids trafficking through late endosomes/lysosomes, like LBPA, cholesterol, sphingomyelin and glycosphyngolipids. Besides this, since vacuoles may reflect a disorder in fluid phase endocytosis, we studied the effect of amiodarone on the traffic of a non-degradable sugar. Finally we correlated the physico-chemical properties of amiodarone analogues with effects on the distribution of LBPA and on the ability to degrade imported proteins. In particular the analogues studied included dronedarone, an amiodarone derivative recently introduced in clinical practice [27].

We found that amiodarone, at concentrations close to patient serum levels, interferes with late compartments of the endocytic pathway blocking the progression of fluid phase endocytosis and causing the inappropriate fusion of organelles, the collapse of lumenal structures, the accumulation of undegraded substrates and the amassing of lipids. These changes recall the Niemann-Pick type C (NPC) phenotype, but originate through a different mechanism, since they are not alleviated by cholesterol removal, while cells treated with NPC-phenotype inducer U18666A revert to the normal after reduction of the cholesterol load. Studies with analogues indicate that high water-solubility at acidic pH is a crucial requirement for the interference with late endosomes/lysosomes and that, in this respect, dronedarone is at least as potent as amiodarone.

## 2. Materials and methods

### 2.1. Cells

BHK and Vero cells, obtained from the European Collection of Cell Cultures (ECACC) and human fibroblasts obtained from normal skin biopsies, were grown in Dulbecco's Modified Eagle's medium (DMEM) supplemented with 10% fetal calf serum, 50 U/ml penicillin, 50 μg/ml streptomycin (all from Sigma–Aldrich, Saint Louis, MO). K562 cells, obtained from ECACC, were grown in RPMI medium, 10% fetal calf serum, 50 μg/ml streptomycin, 50 U/ml penicillin(all from Sigma–Aldrich). Rabbit alveolar macrophages obtained by bronchoalveolar lavage and circulating monocytes obtained from healthy blood donors were cultured in Ringer buffer (145 mM NaCl, 5 mM KCl, 1 mM $MgCl_2$, 2 mM $Na_2HPO_4$, 10 mM glucose, 10 mM HEPES, pH 7.4) plus 0.1% bovine serum albumin (Sigma–Aldrich) as previously reported [28]. Human embryonic kidney cells stably transduced to express the simian virus 40 T antigen (293T), were kindly provided by Prof. D. Baltimore (Rockefeller University, New York, NY, USA). Cell viability was tested with trypan blue exclusion or with an assay based on the reduction of a tetrazolium salt (Cell Proliferation Kit 1[MTT], Roche Diagnostics, Mannheim, Germany). Data presented are from cells >95% viable with respect to control cells.

### 2.2. Plasmids

pEGFP-LC3, source Dr Taamotsu Yoshimori, was from Addgene (Cambridge, MA). eEGF-Rab7 was a kind gift from Dr Robert Lodge(Laval University, Quebec City, Canada). eGFP-Rab5 was from Addgene. pΔenv1 plasmid contains Gag/Pol and Rev encoding sequences of the feline immunodeficiency virus (FIV), p34TF10 strain (GenBank accession no. NC_001482) [29]. pSVC21 construct contains a complete HIV-1 provirus, molecular clone HXBc2 [30]. Transfections were done using Attractene Transfection Reagent from Qiagen (Milan, Italy) according to a protocol provided by the supplier or the calcium phosphate procedure.

**Table 1**
Physicochemical properties of amiodarone and analogues

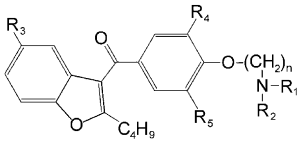

| Compound | MW | *N* | $R_1$ | $R_2$ | $R_3$ | $R_4$ | $R_5$ | pKa[a] | Aqueous solubility of hydrochloride salt | |
|---|---|---|---|---|---|---|---|---|---|---|
| | | | | | | | | | At pH 5.0 (μM) | At pH 7.4 (μM) |
| AMI | 645.3 | 2 | $C_2H_5$ | $C_2H_5$ | H | I | I | 8.47 | 2.04[b] | 0.016[b] |
| MDEA | 617.3 | 2 | H | $C_2H_5$ | H | I | I | 9.40 | 12.0[b] | 0.11[b] |
| DIPAM | 673.4 | 2 | $CH(CH_3)_2$ | $CH(CH_3)_2$ | H | I | I | 9.04 | 0.23[b] | 0.014[b] |
| MeAMI | 617.3 | 2 | $CH_3$ | $CH_3$ | H | I | I | 7.92 | 2.21[b] | 0.051[b] |
| MOPAM | 659.3 | 2 |  | | H | I | I | 3.29 | 0.17[b] | 0.015[b] |
| PIPAM | 657.3 | 2 |  | | H | I | I | 5.35 | 2.22[b] | 0.023[b] |
| PYRAM | 643.3 | 2 |  | | H | I | I | 4.96 | 1.86[b] | 0.049[b] |
| DRO | 556.7 | 3 | $(CH_2)_3CH_3$ | $(CH_2)_3CH_3$ | $NHSO_2CH_3$ | H | H | 9.79 | 900 | <0.001[c] |

[a] Calculated pKa value of amino group using Marvin 5.0.7 software available at http://www.chemaxon.com.
[b] Measured at 22 °C in 5 mM $K_2PO_4$ adjusted to pH 5.0 and 7.4 with diluted HCl. Methanol used as cosolvent.
[c] Values available at http://www.patentstorm.us/patents/6939865/description.html.

### 2.3. Antibodies

Mouse antibody anti LBPA (6C4) was from Echelon Biosciences (Logan, UT). Mouse anti α-tubulin was from Sigma–Aldrich. Rabbit anti NPC1 from Novus Biologicals (Littleton, CO). Rabbit anti giantin, and anti EEA1 were from Abcam (Cambridge, UK). Mouse anti LAMP-1 was from Developmental Studies Hybridoma Bank (University of Iowa, IA). Secondary antibodies conjugated with Alexa Fluor 488 or FITC were from Molecular Probes (Eugene, OR) or from Santa Cruz Biotechnology (Santa Cruz, CA).

### 2.4. Amiodarone analogues

Amiodarone was from Sigma–Aldrich. Dronedarone was extracted from Multaq commercial pills (Sanofi-Aventis, Munchenstein, Switzerland). Briefly one Multitaq tablet was dissolved in 25 ml of 1 M $NH_3$ and extracted 3 times with 10 ml of methylene chloride. The organic phase was collected, dried under reduced pressure, dissolved in DMSO and stored at −26 °C. Other analogues used in this study, whose synthesis has been reported previously [31], are presented in Table 1. They included MeAM (2-butyl-benzofuran-3-yl)-4-[2-(dimethylamino-ethoxy)-3,5-diiodophenyl]methanone, DIPAM (2-butyl-benzofuran-3-yl)-4-[2-(diisopropylamino)ethoxy]-3,5-diiodophenyl-methanone·hydrochloride, PYRAM [4-(2-butyl-benzofuran-3-yl)-[3,5-diiodophenyl-4-(2-pyrrolidin-1-yl-ethoxy)phenyl]-methanone·hydrochloride], PIPAM [4-(2-butyl-benzofuran-3-yl)-[3,5-diiodophenyl-4-(2-piperidinoethoxy)phenyl] methanone·hydrochloride], MOPAM [2-n-butyl-3-(3,5-diiodo-4-β-Nmorpholinoethoxybenzoyl)benzofuran]. MDEA·hydrochloride [2-n-butyl-3-(3,5-diiodo-4-ethylaminoethoxybenzoyl)-benzofuran] was a gift from Sanofi-Aventis (Muchenstein, Switzerland).

### 2.5. Other materials and reagents

Shiga toxin 1was a generous gift from Dr. Maurizio Brigotti (Department of Experimental Pathology, University of Bologna, Italy). Surfactant protein A (SP-A) was isolated from the therapeutic lung lavage fluid of patients suffering from alveolar proteinosis and labelled with $^{125}I$ to a specific activity of 400–600 cpm/ng protein, as previously reported [9].

8-Hydroxypyrene-1,3,6-trisulfonic acid (HPTS) and tetramethylrhodamine dextran (10 kDa MW) were from Molecular Probes (Eugene, OR). P-xylene-bis-pyridiniumbromide (DPX) was from Chemie Brunschwig (Basel, Switzerland). DRAQ5™ was from Biostatus Limited (Shepshed, UK). [$^3$H]leucine (specific activity 151.0 Ci/mmol) was from Amersham Pharmacia Biotech (little Chalfont, UK). Hyonic Fluor was from Packard (Groningen, The Netherlands). Benzonase was from Novagen (San Diego, CA). Complete protease inhibitor cocktail was from Roche Diagnostics (Mannheim, Germany). Creatine phosphokinase was from Boehringer (Mannheim, Germany). Lysenin and lysenin antiserum were from Peptide Institute (Osaka, Japan). All other reagents were from Sigma–Aldrich.

### 2.6. Immunofluorescence

Cells adhering to glass coverslips (Falcon, Milan, Italy), after incubation for 1–18 h with different drugs, were fixed with 3% paraformaldehyde (PFA) in PBS for 20 min, quenched with 50 mM $NH_4Cl$ for 15 min, permeabilized with 50 μg digitonin/ml PBS for 5 min, blocked with 0.2% gelatin in PBS for 30 min, incubated with primary antibody for 1 h and then with the appropriate secondary antibody for 30 min. Stained cells were mounted in Vectashield (Vector Laboratories, Burlingame, CA) and analyzed with a Leica TCS SP2 laser-scanning confocal microscope. Dilutions of primary antibodies were: anti LBPA 1/10, anti LAMP-1 1/50, anti giantin 1/50, anti NPC1 1/50. Pictures presented are from at least duplicate experiments.

### 2.7. Morphometry

After staining for LBPA, cells were counterstained with propidium iodide and, from randomly selected cell profiles, LBPA-positive structures were counted and their diameter was measured. Counting and diameter measurement were done in a blind fashion by two independent observers on images obtained

with the confocal resident software. Data presented are from 50 to 150 cells profiles and 250 to 800 LBPA-positive structures for each treatment.

### 2.8. Free cholesterol visualization with filipin

Cells were fixed with 3% PFA for 30 min, quenched with 50 mM $NH_4Cl$ for 7 min, incubated for 2 h with 250 μg filipin/ml 0.2% BSA in PBS, mounted with 10% glycerol/PBS and then analyzed with a Leica DMR epifluorescence microscope.

### 2.9. Staining of sphingomyelin

Sphingomyelin was stained using lysenin, a 41 kDa pore-forming toxin from *Eisenia foetida* which binds sphingomyelin [32,33]. Briefly, cells adhering to glass coverslips, were fixed, quenched and permeabilized as reported in Section 2.6 and then were blocked with 0.2% gelatin/PBS for 30 min. Afterwards cells were incubated on ice for 1 h with 1 μg/ml lysenin in 0.2% gelatin/PBS, rinsed extensively with PBS at room temperature, incubated for 1 h with antibody anti-lysenin (1/1000) and anti LBPA (1/10) in 0.2% gelatin/PBS, exposed to the appropriate secondary antibodies for 30 min and then were mounted and analyzed by confocal microscopy.

### 2.10. BODIPY-lactosylceramide transport

Trafficking of glycosphingolipids was analyzed using boron-dipyrromethenelactosylceramide (BODIPY-LacCer, Molecular Probes, Eugene, OR) as reported [34]. Briefly, after rinsing with DMEM, BHK cells were incubated at 37 °C for 45 min with 8 μM BODIPY-LacCer/albumin complex in 1% FBS/DMEM to allow internalization and trafficking to late endosomes. Subsequently, after extensive rinsing, cells were incubated at 37 °C for 1 more hour with 1% FBS/DMEM to allow accumulation of BODIPY-LacCer in the Golgi. Afterwards cells were back-exchanged 6 times with 5% fatty acid free albumin/DMEM at 10 °C and then were analyzed with a Leica DMR epifluorescence microscope or with a confocal microscope.

### 2.11. Dextran uptake

Adhering BHK cells were incubated for 12 h with tetramethylrhodamine dextran (3 mg/ml in DMEM/10%FBS/antibiotics) in the absence or in the presence of 10 μM amiodarone. Afterwards, after extensive rinsing, cells were chased with plain medium (controls) or 10 μM amiodarone for 5 h, a time sufficient, in control cells, for the transfer of uptaken dextran to the lysosomes [35]. At the end, after staining of the nuclei with 5 μM DRAQ5™, LBPA was evidenced as reported in "Immunofluorescence" and cells were analyzed by confocal microscopy.

### 2.12. Effect of amiodarone and analogues on the degradation of surfactant protein A (SP-A)

SP-A, a component of lung surfactant, besides regulating surfactant turnover, binds viruses and bacteria present in the alveoli and presents them to alveolar macrophages that then destroy both infectious agent and SP-A into lysosomes [36]. To compare the effect of amiodarone and analogues on the degradation of SP-A, $2 \times 10^6$ rabbit alveolar macrophages in 1 ml Ringer buffer, 1 mg/ml bovine serum albumin, 50 U/ml penicillin, 50 μg/ml streptomycin, were incubated for 1 h with 0–50 μM amiodarone or analogue and then for one more hour with 1 μg/ml $^{125}$I-SP-A in the continuous presence of amiodarone or amiodarone analogue. At the end the radioactivity soluble in 20% cold trichloroacetic acid was measured and results were expressed as percent of degradation by control cells. $ID_{50}$ (concentration resulting in 50% inhibition) was calculated, using only data from cells over 95% viable by trypan blue exclusion.

### 2.13. Transferrin recycling

Transferrin (Tf) recycling was measured as reported [37]. Adhering blood monocytes in RBA ($2 \times 10^6$ cells/well) were incubated for 1 h at 37 °C with 4 μg/ml $^{125}$I-Tf in the absence or in the presence of 10 μM amiodarone, to reach equilibrium labelling. Cells were then rinsed with ice-cold PBS and surface bound Tf was removed first by incubation for 15 min at 4 °C with 50 μM deferoxaminemesylate in 150 mM NaCl, 2 mM $CaCl_2$, 20 mM Na acetate pH 5.0 and then by incubation for 20 min at 4 °C with 50 μM deferoxaminemesylate and 125 nM human apotransferrin in PBS. Subsequently cells were rinsed again with ice-cold PBS and triplicate cultures were incubated at 37 °C for 0, 5 or 10 min with prewarmed RBA containing 50 μg/ml unlabelled human Tf, and 0 or 10 μM amiodarone. At the end cells were rinsed with ice-cold PBS, lysed with 1 N NaOH and on the lysate radioactivity was measured using Hyonic Fluor (Packard) and proteins were measured with the Bradford method. Tf recycled was expressed as % of radioactivity lost from cells with respect to time 0.

### 2.14. Shiga toxin 1 cytotoxicity assay

Vero cells in DMEM/10%FBS adhering to 24-well plates (Falcon, Milan, Italy) at a density of $10^5$ cells/well were incubated for 3 h with Shiga toxin 1 (0–50 ng/ml) in the presence of 0–20 μM amiodarone and then for 30 min with [$^3$H]leucine in PBS (200 nCi/well). At the end cells were washed 1 time with 50% methanol, fixed for 30 min with cold 100% methanol and then washed 3 times with 10% cold trichloroacetic acid (TCA). The final precipitate was dissolved with 1 N NaOH and the lysate was used for protein assay and radioactivity counting. The activity of Shiga toxin 1 was expressed as the decrease in the incorporation of [$^3$H]leucine into acid-precipitable material.

### 2.15. Amiodarone effect on lentiviral particle release

293T cells ($1.5 \times 10^6$) were seeded into 25 cm$^2$ flasks (Falcon, Milan, Italy) and, twenty-four hours later, were transfected by calcium phosphate method with 1.25 μg of the appropriate viral construct (pΔenv1 or pSVC21). The total amount of DNA was brought to a total of 8 μg by adding an empty vector (pBluescriptKSþ, Stratagene, La Jolla, CA). Two hours prior transfection the cells were treated with 0 or 10 μM amiodarone that was maintained till VLP harvesting. Twenty-four hours post-transfection the culture supernatants were collected and cells were lysed in radioimmunoprecipitation assay (RIPA) buffer [140 mM NaCl, 8 mM $Na_2HPO_4$, 2 mM $NaH_2PO_4$, 1% Nonidet P-40, 0.5% sodium deoxycholate, 0.05% sodium dodecyl sulfate (SDS) pH 8.0]. Culture supernatants were clarified by low speed centrifugation and passaged through 0.46 μm-pore-size filters. Released VLPs, brought to 4 °C, were deposited over a 20% sucrose cushion and centrifuged at 27,000 rpm for 2 h in a Beckman SW41 rotor. Pelleted VLPs were then lysed in RIPA buffer. In order to examine intracellular GAG expression levels and virus-like particles (VLP) release, cell and VLP lysated were subjected to SDS-polyacrylamide gel electrophoresis and resolved proteins were electroblotted onto Hybond-C-Extra membranes (Amersham Pharmacia Biotech, Milan, Italy). Membranes were then incubated with the appropriate antibody, namely a monoclonal anti-FIV capsid antiserum (anti FIV-p24 Gag, Serotec, Dusseldorf, Germany) or a rabbit anti CA-polyclonal antiserum (Advanced

Biotechnologies, Columbia, Maryland, USA) followed by the appropriate peroxidase-conjugated secondary antibody. The blots were developed with enhanced chemiluminescence reagents (Amersham Pharmacia Biotech, Milan, Italy).

### 2.16. Exosome release

Exosome secretion was estimated by measuring acetylcholinesterase activity released by K562 cells, an erytroleukemia cell line of human origin [38]. Briefly, 20–25 × $10^6$ K562 cells were incubated for 8 h in 10 ml RPMI medium/10% FBS/antibiotics and 0, 2 or 10 μM amiodarone. At the end the medium was collected on ice, centrifuged at 800 × *g* for 10 min to sediment cells and then at 12,000 × *g* for 30 min to sediment debris. Exosomes were sedimented from the remaining supernatant by centrifugation at 100,000 × g for 2 h. The exosome pellet was washed with PBS and then suspended in 100 μL PBS, 0.1% Triton X 100. Fifty μL of that suspension were then incubated for 45 min at 37 °C with 1.25 mM acetylthiocholine, 0.1 mM 5,5′-dithiobis(2-nitrobenzoic acid), 120 mM NaCl, 5 mM KCl, 4 mM $KH_2PO_4$, 16 mM $Na_2HPO_4$, 0.5 mM $CaCl_2$, 1.0 mM $MgCl_2$, pH 7.4 (final volume 1 ml) and the change in absorbance was followed continuously. After correction for spontaneous degradation of substrate, enzymatic activity was normalized to the number of cells used and expressed as % of activity liberated by control cells. Viability at end incubation, analyzed by trypan blue exclusion, was >97% both for control and amiodarone treated cells.

### 2.17. Statistical analysis

Data are presented as means ± SE. Paired "*t*" test was used to analyze differences between means of paired samples. Single factor ANOVA was used to analyze differences between several groups, using the Newman–Keuls test for data normally distributed and the Dunn test for data not normally distributed. 0.05 was the level of significance accepted.

## 3. Results

### 3.1. Amiodarone and its main metabolite MDEA cause fusion of LBPA-rich organelles; the change is cytoskeleton-dependent and reversible

Clinical experience indicates that patients treated with amiodarone display inclusion bodies filled with membranous structures in different cell types [7,9,28] and accumulate in the airways LBPA, a poorly degradable phospholipid present in the internal membranes of late endosomes [12,15]. Since the effect of amiodarone on the distribution of LBPA at the cell level has never been studied, BHK cells were incubated with 0–10 μM amiodarone for 16 h and the distribution of LBPA was analyzed by confocal microscopy. As shown in Fig. 1A, in control cells LBPA presented as puncta with a juxtanuclear distribution, consistent with its association with late endosomes. In the presence of amiodarone, LBPA-positive structures decreased in number, increased in diameter and changed distribution from juxtanuclear to peripheral (Fig. 1A). Quantitative analysis indicated that the change in number and diameter of LBPA-positive structures was concentration dependent and was significant at 2 μM amiodarone, a concentration commonly found in the serum of chronically treated patients (Fig. 1B). MDEA, the main metabolite of amiodarone, which reaches serum concentrations close to those of the parent drug [8], was more powerful than amiodarone and the combination 2 μM amiodarone plus 2 μM MDEA, affected LBPA distribution similarly to 10 μM amiodarone (Fig. 1A, B). The effect on the distribution of LBPA was reproducible. In 5 independent experiments in which cells were incubated with 10 μM amiodarone for 16 h, the number of LBPA-rich structures per cell profile decreased by 69.0 ± 4.5% and their diameter increased by 42.6 ± 5.2% ($p < 0.01$ for both differences).

As shown in Fig. 2, the effect of amiodarone was reversible, since BHK cells incubated for 16 h with 10 μM amiodarone and then with plain medium for further 16 h, regained their normal LBPA distribution. Fig. 2 also shows that changes in the distribution of LBPA were attenuated by inhibiting microtubule polymerization with nocodazole and could be prevented by treatment with ammonium chloride. Since alkalinization inhibits the accumulation of amiodarone, while nocodazole has no effect on the association of amiodarone with target cells [6,7], we conclude that: (a) amiodarone induces fusion of organelles rich in LBPA, (b) the process is cytoskeleton-dependent and reversible, (c) alkalinization prevents fusion by inhibiting the accumulation of amiodarone within target cells, (d) although amiodarone increases the pH of acidic organelles [6], lumenal alkalinization by itself has no role in the re-distribution of LBPA, (f) the effect on LBPA distribution suggests that amiodarone interferes with late compartments of the endocytic pathway. Since 10 μM amiodarone had effects similar to those of 2 μM amiodarone plus 2 μM MDEA, typically found in patient sera, in most of the following experiments cells were incubated with 10 μM amiodarone for 16 h, a time sufficient for the development of the amiodarone-induced phenotype.

### 3.2. Structural determinants of amiodarone interference with the endocytic pathway

To clarify the structural basis of the interference of amiodarone with late endosomes/lysosomes, we analyzed the effects of amiodarone analogues (Table 1) on the distribution of LBPA and on the degradation of imported proteins. The analogues, obtained by modification of the lateral group diethylamino-β-ethoxy, were used under conditions that did not influence cell viability.

To study the effects on the distribution of LBPA, BHK cells were incubated for 16 h with 10 μM amiodarone or analogue and then number and diameter of LBPA-positive structures were analyzed by confocal microscopy. To study the effects on the degradation of imported proteins, rabbit alveolar macrophages were incubated for 1 h with 0–50 μM amiodarone or analogue and then, for a further hour, with 1 μg/ml $^{125}$I-Surfactant Protein A (SP-A) in the continuous presence of amiodarone or analogue. At the end water-soluble radioactivity was measured and $ID_{50}$ (concentration of analogue resulting in 50% inhibition with respect to degradation by control cells) was calculated. SP-A is a calcium-dependent lectin secreted in the alveoli by lung type 2 cells, which, besides regulating the life-cycle of lung surfactant phospholipids, binds viruses and bacteria and mediates their uptake and destruction by alveolar macrophages [39]. We previously found that amiodarone inhibits the degradation of SP-A by lung cells both *in vitro* and *in vivo* [9].

As shown in Table 2 the effects on the degradation of SP-A and on the distribution of LBPA were to a good extent concordant, since compounds with the greatest ability to inhibit the degradation of SP-A (amiodarone or MeAMI) also had the greatest impact on number and size of LBPA-positive structures. On the opposite, compounds with the lowest activity on SP-A degradation (DIPAM or MOPAM), had the weakest effect on the distribution of LBPA. Trying to correlate chemico-physical properties and activity, the best results were obtained by arranging compounds according to the product pKa × water-solubility at pH 5.0. In fact, as shown in Table 2, compounds with the highest value of this product (MeAMI or amiodarone) had the strongest effect on the degradation of SP-A and on the distribution of LBPA, while compounds with the lowest value (DIPAM or MOPAM) had little effect. From Table 2 it also

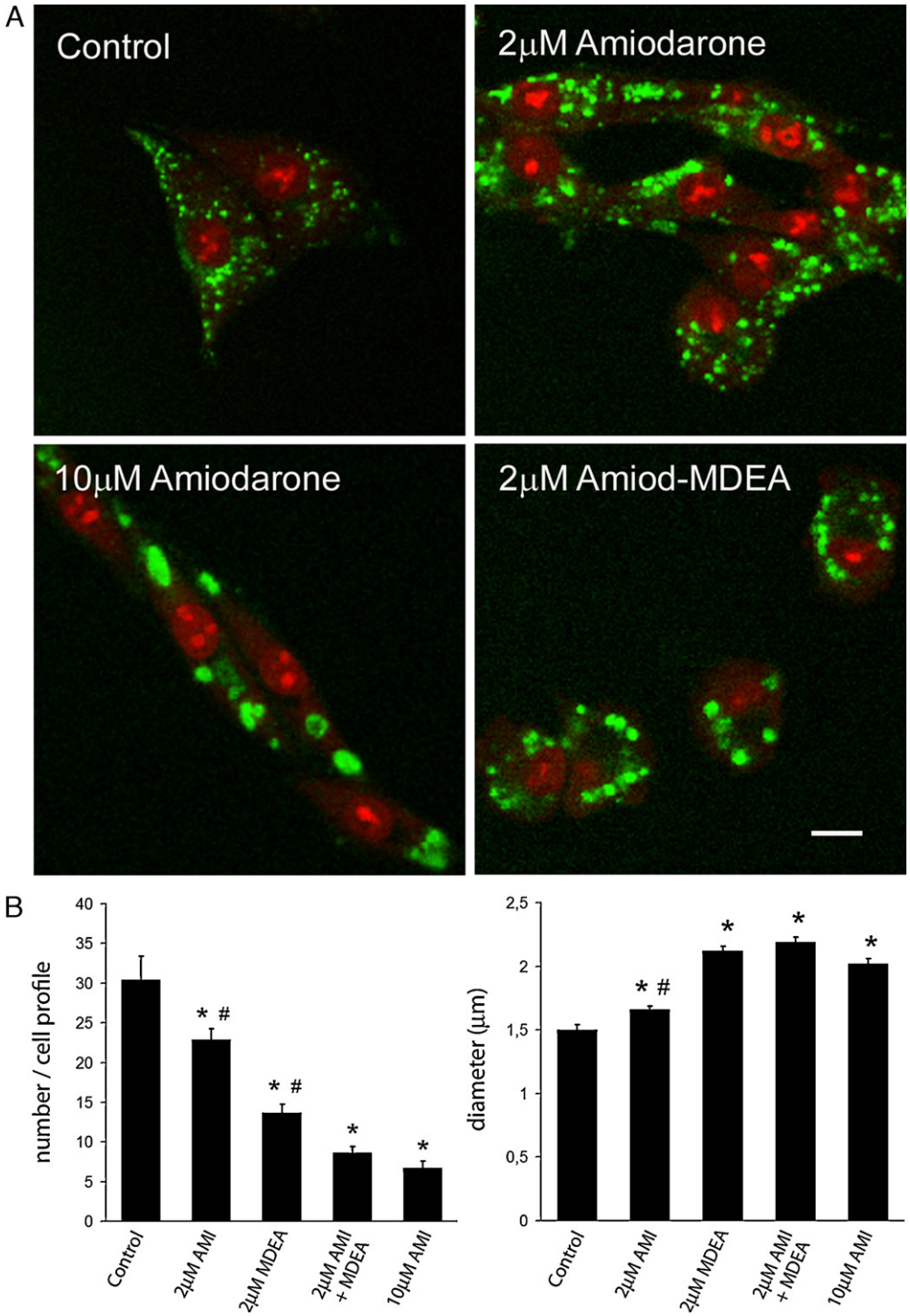


**Fig. 1.** Amiodarone and monodesethylamiodarone induce fusion of organelles containing lysobisphosphatidic acid. (A) BHK cells were incubated with amiodarone or monodesethylamiodarone (MDEA) for 16 h and the distribution of lysobisphosphatidic acid (LBPA) was analyzed by confocal microscopy. (B) Morphometry from confocal images: effect of amiodarone and MDEA on number and diameter of LBPA-positive organelles. $M \pm$ SE. *Different from control, # different from 10 μM amiodarone ($p < 0.05$, ANOVA). Bar 10 μm.

appears that a basic pKa by itself cannot account for the observed effects, since DIPAM, which ranked towards the top for pKa, but had low water-solubility at acidic pH, had no effect on the degradation of SP-A or the distribution of LBPA.

On the whole these data support the view that the interference with the endocytic pathway depends on the ability to accumulate within acidic organelles and agree with recent evidence indicating that the accumulation of weakly basic amines into acidic organelles depends on high pKa and on a low propensity, in the ionized state, to diffuse back through the organellar limiting membrane [40]. In agreement with this interpretation, MDEA, which, considering the product pKa × solubility in water at pH 5.0, ranks higher than amiodarone, had a stronger effect on the distribution of LBPA (Fig. 1) and inhibited the degradation of SP-A with a slightly lower $ID_{50}$ value ($10.4 \pm 1.7$ μM) ($N = 3$). A further implication from the present data is that amiodarone target might be located into or might be accessible from the lumen of late endosomes/lysosomes.

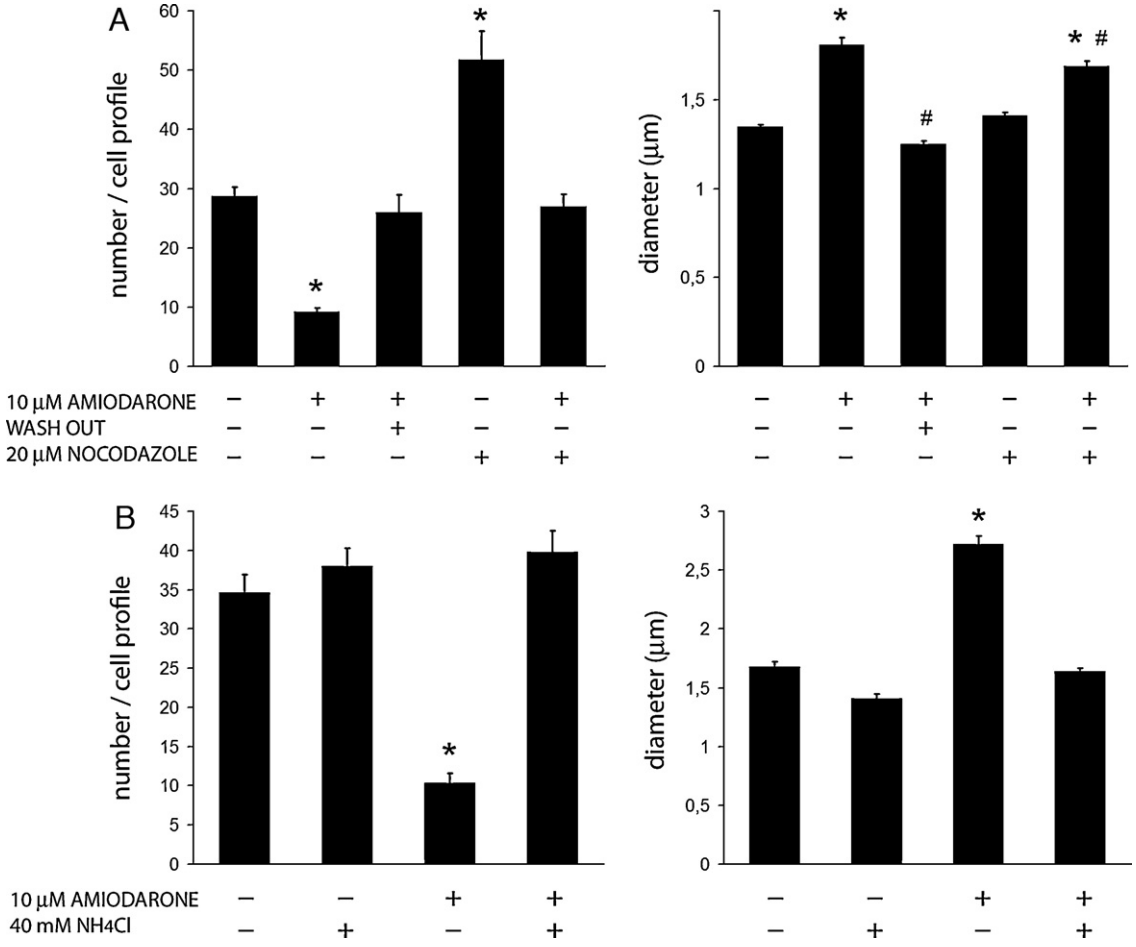


**Fig. 2.** Fusion of LBPA-rich organelles induced by amiodarone is reversible, cytoskeleton-dependent and inhibited by alkalinization. (A) BHK cells incubated for 16 h with 10 μM amiodarone and then with plain medium (wash out) or for 16 h with 10 μM amiodarone in the presence of nocodazole. (B) BHK cells incubated for 16 h with 10 μM amiodarone without or with ammonium chloride. In both experiments number and diameter of LBPA-positive organelles were derived from confocal images. $M \pm SE$. *Different from control, # different from 10 μM amiodarone ($p < 0.05$, ANOVA).

**Table 2**
Relationship between physicochemical properties of amiodarone analogues and effects on the degradation of surfactant protein A (SP-A) and on cell distribution of LBPA.

| Compound[a] | pKa × solubility in water at pH 5.0 | SP-A degradation $ID_{50}$[b] (μM) | LBPA-positive structures[c,d] | |
|---|---|---|---|---|
| | | | Diameter (μm) | N°/cell profile |
| MeAMI | 17.50 | 11.2 ± 1.0 | 2.45 ± 0.08 | 4.5 ± 0.6 |
| Amiodarone | 17.28 | 13.4 ± 2.1 | 2.01 ± 0.03 | 5.2 ± 0.4 |
| PIPAM | 11.88 | 22.8 ± 7.2 | 1.73 ± 0.03 | 14.7 ± 2.1 |
| PYRAM | 9.22 | 23.8 ± 10.2 | 2.08 ± 0.05 | 7.6 ± 0.6 |
| DIPAM | 2.07 | >50.0 | 1.64 ± 0.04 | 24.6 ± 3.0 |
| MOPAM | 0.55 | >50.0 | 1.45 ± 0.02 | 29.3 ± 0.6 |

[a] Compounds arranged in order of decreasing value of the product (pKa × solubility in water at pH 5.0).
[b] Degradation of SP-A measured as TCA-soluble radioactivity released by rabbit alveolar macrophages during 1 h incubation with 1 μg/ml $^{125}$I-SPA. $ID_{50}$ = analogue concentration needed to decrease degradation to 50% of control. $M \pm SE$, data from 3 to 13 experiments.
[c] BHK cells were incubated for 16 h with 10 μM analogues and distribution of LBPA was analyzed by confocal microscopy. Data from 50 to 130 cells and 200 to 800 organelles.
[d] In control cells LBPA-positive structures were 28.6 ± 1.1/cell profile, and diameter was 1.46 ± 0.02 μm. $M \pm SE$.

### 3.3. Amiodarone changes the distribution of unesterified cholesterol, glycosphingolipids and sphingomyelin

In Niemann-Pick type C disease, the accumulation of LBPA is a facet of a more general disturbance in the traffic of cell lipids [20,41]. We speculated that this might hold true also for cells treated with amiodarone. To explore this possibility, we incubated BHK cells with 0–10 μM amiodarone for 16 h and then analyzed the distribution of unesterified cholesterol, glycosphingolipids and sphingomyelin.

Unesterified cholesterol was detected by staining fixed cells with the fluorescent polyene antibiotic filipin [42]. As shown in Fig. 3, in control BHK cells unesterified cholesterol was associated with small vesicles mostly distributed around the nucleus, while in the presence of amiodarone it associated with larger structures. The change, clearly discernible in the presence of 2 μM amiodarone, reached full expression in the presence of 10 μM amiodarone, giving to cells an appearance similar to that induced by 10 μM U18666A, a known inducer of the NPC phenotype (Fig. 3) [18]. Besides changing the distribution of unesterified cholesterol,

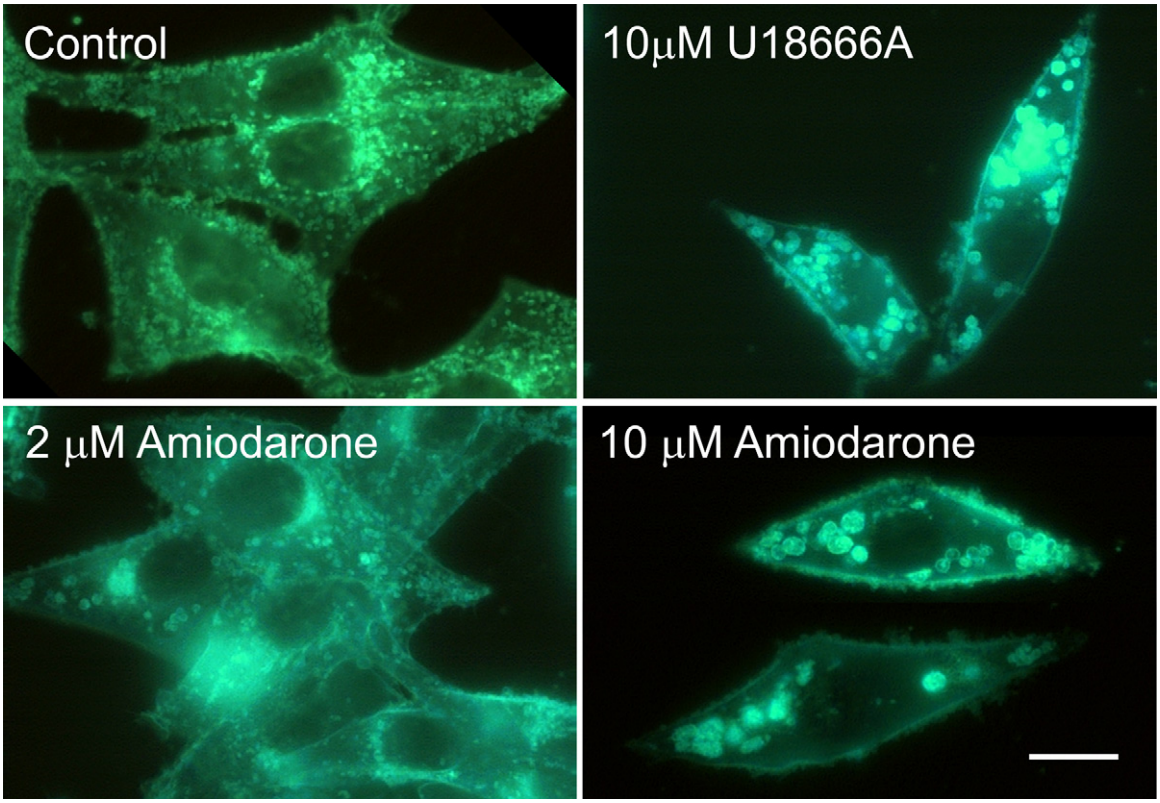


**Fig. 3.** Amiodarone and U18666A alter the distribution of unesterified cholesterol. BHK cells were incubated for 16 h with plain medium, 2 or 10 μM amiodarone or 10 μM U18666A, stained with filipin and analyzed by epifluorescence microscopy. Bar 10 μm.

amiodarone also changed cell cholesterol content. In fact, after 16 h incubation with 10 μM amiodarone, cell cholesterol increased by 17.3 ± 5.2% ($p = 0.03$, paired "$t$" test, $N = 5$), while the ratio between total and unesterified cholesterol did not change.

To study the distribution of sphingomyelin BHK cells were exposed to 0–10 μM amiodarone, fixed and then incubated first with lysenin, a sphingomyelin-binding protein isolated from the coelomic fluid of the earthworm *Eisenia foetida* [32,33] and then with an anti-lisenin antiserum, followed by a fluorescent secondary antibody. As shown in Fig. 4, in control cells sphingomyelin was associated with the plasma membrane and with organelles close to the plasma membrane and was rigorously separated from LBPA. Cells treated with 2 μM amiodarone and 10 μM U18666A displayed a more intense staining with respect to control cells. Besides this, in cells treated with 10 μM amiodarone, sphingomyelin tended to distribute as clumps, associated with complex internal structures and, at some places, co-localized with LBPA. The reason of the increased staining intensity in treated cells remains unclear. Possibly amiodarone and U18666A rendered plasma membrane sphingomyelin more accessible to lysenin.

Distribution and trafficking of glycosphingolipids was analyzed by incubation of BHK cells with BODIPY-LacCer, a sphingolipid analogue in which the naturally occurring fatty acid moiety is replaced with N-[5-(5,7 dimethyl boron dipyrromethanedifluoride)-1-pentanoic acid]. Cells were allowed to internalize BODIPY-LacCer for 45 min to allow loading of late endosomes, followed by 1 h chase to accumulate the fluorescent probe in the Golgi and then were analyzed by confocal microscopy [34]. As shown in Fig. 5A, in control cells BODIPY-LacCer accumulated in juxtanuclear structures compatible with the Golgi, while in amiodarone treated cells it accumulated in round structures lacking the staining pattern typical of the Golgi system. Fig. 5A also shows that amiodarone did not perturb the Golgi organization, since it did not change the distribution of the specific marker giantin. Furthermore it appears that the change in BODIPY-LacCer distribution induced by amiodarone (formation of large cytoplasmic aggregates) was different from the distribution as scattered cytoplasmic dots observed in the presence of 10 μM U18666A (Fig. 5B). Co-localization studies between BODIPY-LacCer and specific Golgi markers were hindered by the fact that BODIPY-LacCer exhibits a concentration dependent shift in its fluorescence emission from green to red wavelengths as a result of excimer formation at high concentrations [36]. From these data we conclude that amiodarone alters the cell distribution of sterols, phospholipids, sphingolipids and glycosphingolipids, generating a phenotype with partial resemblance with Niemann-Pick type C disease [19,20,43].

### *3.4. Cholesterol removal alleviates the change in LBPA distribution induced by U18666A, but not that induced by amiodarone*

In NPC disease accumulating lipids are connected both spatially and functionally and alleviation of the phenotype can be obtained by decreasing cholesterol levels with sterol-binding agents like methyl-β-cyclodextrin [21], by inhibiting glycosphingolipid synthesis with 1-deoxynojirimycin [22] or by increasing lipid degradation through overexpression of acid sphingomyelinase [23]. In particular LBPA accumulation can be attenuated by treatment with methyl-β-cyclodextrin [21,41,42,44–46].

To clarify the mechanism of lipid accumulation due to amiodarone, BHK cells were loaded for 24 h with 1 mM methyl-β-cyclodextrin, rinsed extensively, incubated for further 16 h with plain medium, 10 μM amiodarone or 10 μM U186662 and then processed for confocal microscopy and analysis of LBPA distribution. Results were compared with those of cells not treated with methyl-β-cyclodextrin. As shown in Fig. 6, in cells not treated with methyl-β-cyclodextrin amiodarone and U18666A had similar effects, decreasing the number and increasing the diameter of LBPA-positive structures. On the opposite, pre-treatment with

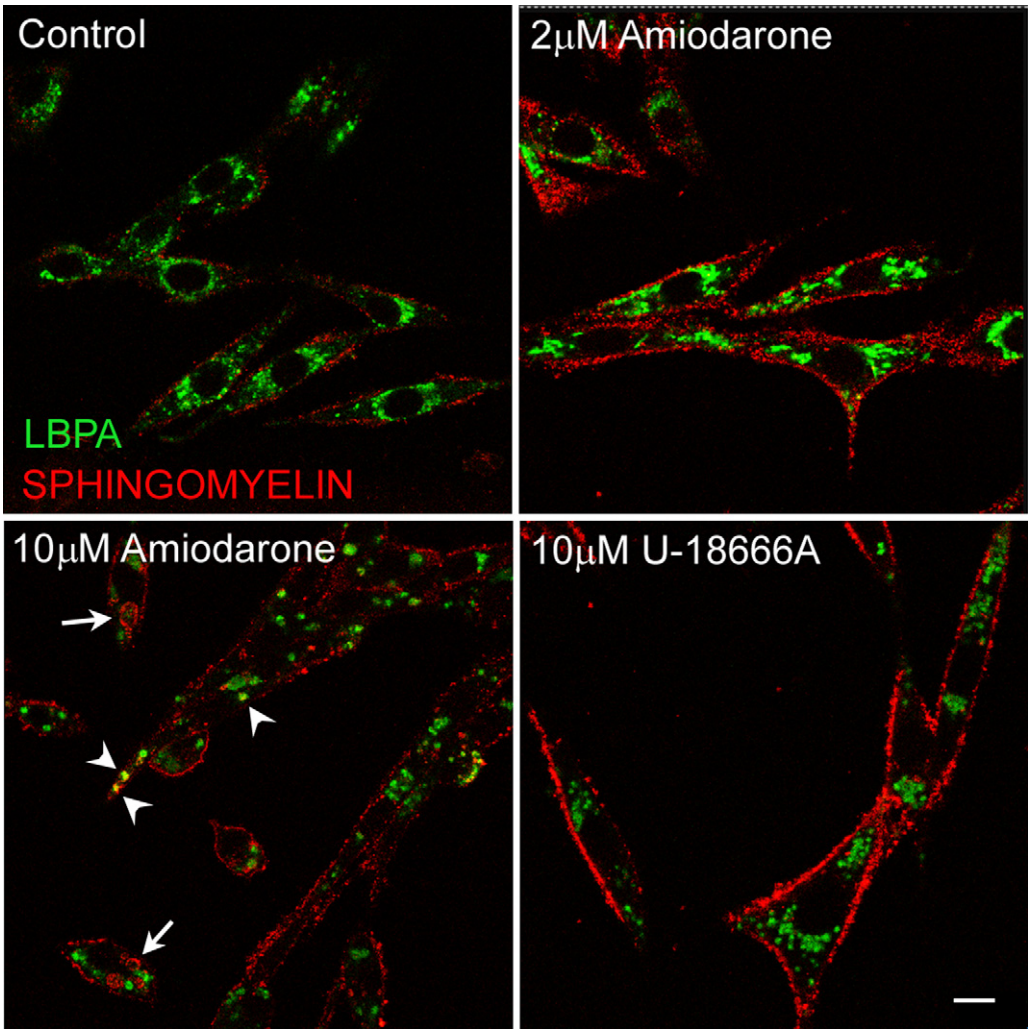


**Fig. 4.** Amiodarone changes the distribution of sphingomyelin. BHK cells, exposed for 16 h to control medium, 2 or 10 μM amiodarone or 10 μM U18666A, were fixed, incubated first with the sphingomyelin-binding protein lysenin and then with antibodies to lysenin and LBPA. After incubation with secondary antibody cells were analyzed by confocal microscopy. Red, sphingomyelin; green, LBPA. Arrows indicate sphingomyelin in intracellular structures. Arrowheads indicate co-localization of sphingomyelin and LBPA (yellow). Bar 10 μm.

methyl-β-cyclodextrin increased the diameter of the aggregates of LBPA induced by amiodarone, worsening the phenotype, but decreased the diameter and increased the number of aggregates of LBPA induced by U18666A, alleviating the phenotype (Fig. 6). From these data we conclude that changes induced by amiodarone do not strictly recapitulate the NPC phenotype.

### *3.5. Vacuoles induced by amiodarone are caused by interference with fluid phase endocytosis*

Dextrans are polysaccharides with good water solubility, low toxicity and resistance to cleavage by most endogenous cell glycosidases and thus represent ideal tracers to study the progress of membrane-impermeable cargo along the endocytic pathway. After uptake, dextrans move through the endocytic pathway ending up into lysosomes, from where they are returned to the extracellular milieu. Wild type fibroblasts in one day may dispose of up to 80% of uptaken dextran [18]. To study the effect of amiodarone on the trafficking of dextran along the endocytic pathway, BHK cells were loaded with tetramethylrhodamine dextran in the absence or in the presence of 10 μM amiodarone and then were chased for 5 h with plain medium or in the presence of 10 μM amiodarone, a time sufficient in control cells to move all visible dextran to the lysosomes [35]. As shown in Fig. 7, in control cells uptaken dextran had a point-like distribution. On the opposite, cells loaded with TMR-dextran and then chased in the continuous presence of amiodarone, retained a greater fraction of uptaken dextran, which was associated with swollen organelles. At some places these organelles also contained LBPA. From these data we conclude that amiodarone may cause the formation of vacuoles by interfering with the progression of fluid phase endocytosis. Furthermore, the co-localization of LBPA and dextran in swollen organelles suggests that accumulation of water-soluble materials may contribute also to the widening of inclusion bodies.

### *3.6. Amiodarone affects diverse but not all subsets of organelles pertaining to late endosomes/lysosomes*

In agreement with previous observations that amiodarone affects late compartments of the endocytic pathway [6,7], we found that the abnormal structures induced by amiodarone exhibit late endosomal markers like LAMP1, Rab7 and NPC1, but not markers of early endosomes. Indeed, the distribution of transiently expressed GFP-Rab5 did not change after exposure to amiodarone (Fig. 1SA). On the opposite, as shown in Figs. 8 and 9 and 1SB, in control cells LAMP1 presented as puncta distributed around the nucleus, while after incubation with 2 or 10 μM amiodarone it

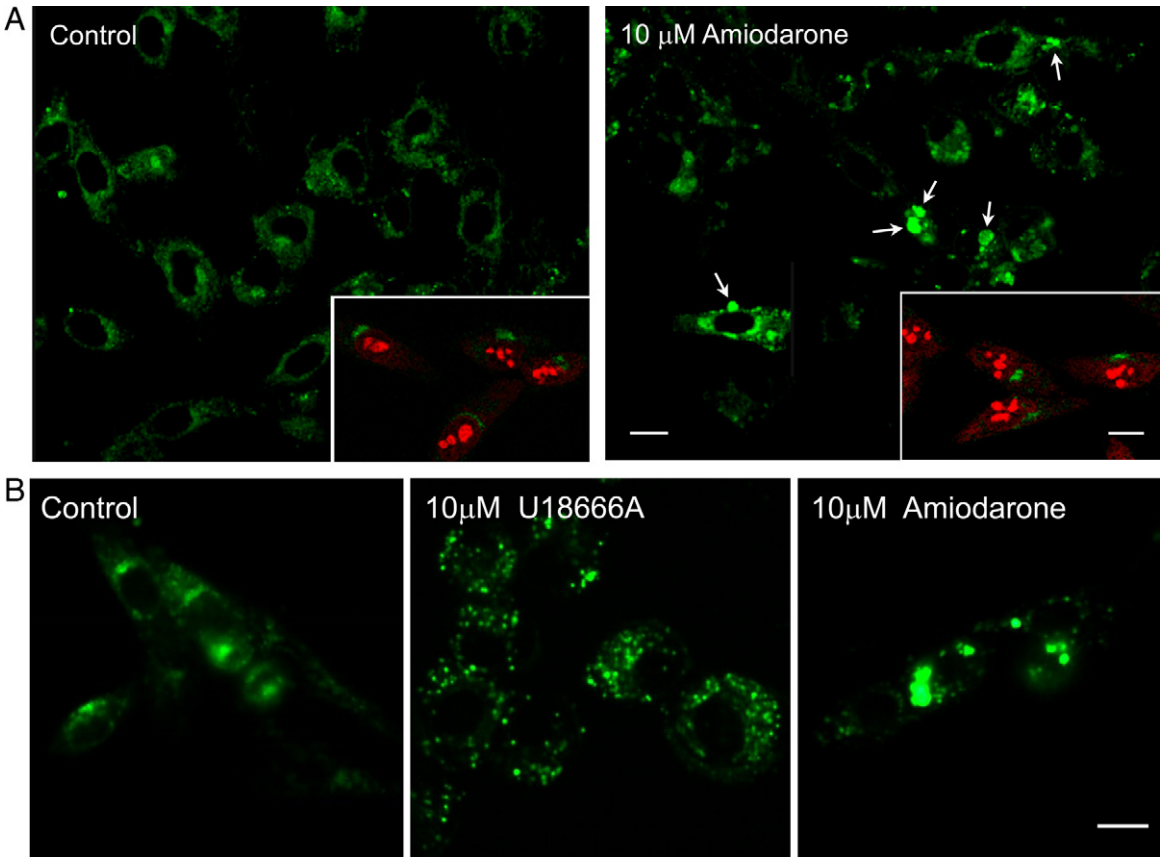


**Fig. 5.** Amiodarone alters the traffic of glycosphingolipids. (A) BHK cells, exposed for 16 h to control medium or 10 μM amiodarone were incubated for 45 min with BODIPY-LacCer, chased for one further hour and then analyzed by confocal microscopy. Inset: distribution of the Golgi marker giantin (green) in cells whose nuclei were stained red with propidium. Arrows: abnormal collections of BODIPY-LacCer in amiodarone-treated cells. (B) Trafficking of BODIPY-LacCer in BHK cells exposed for 16 h to control medium, 10 μM amiodarone or 10 μM U18666A and then analyzed by epifluorescence microscopy. Bar 10 μm.

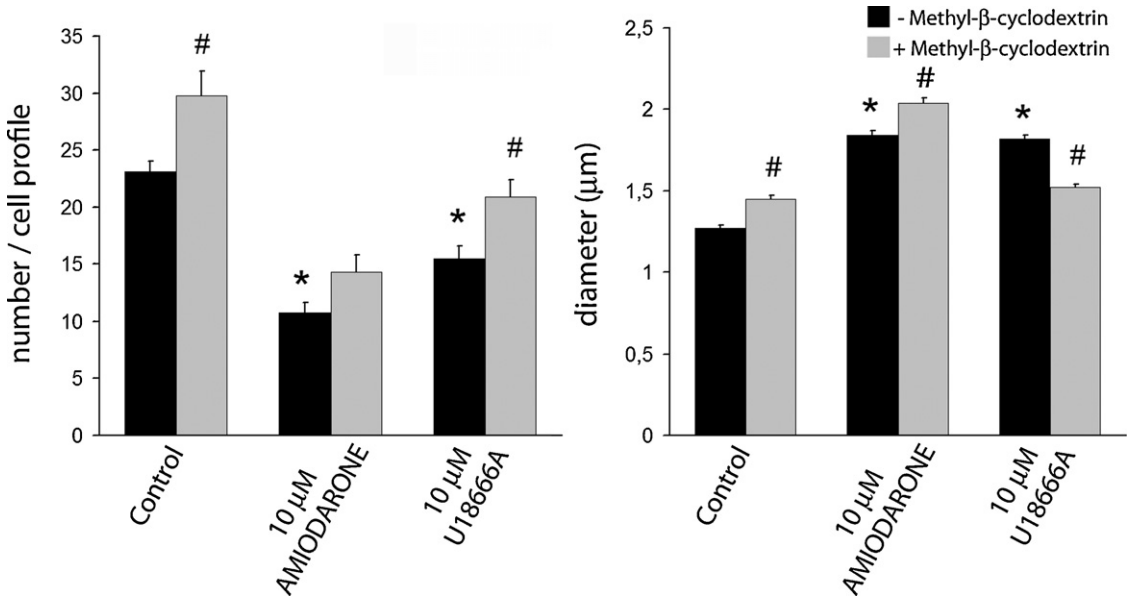


**Fig. 6.** Cholesterol removal alleviates the change in LBPA distribution induced by U18666A, but not that induced by amiodarone. BHK cells were incubated for 24 h with control medium or 1 mM methyl-β-cyclodextrin and then for further 16 h with control medium, 10 μM amiodarone or 10 μM U18666A. At the end the distribution of LBPA was analyzed by confocal microscopy and number and diameter of LBPA-positive structures were measured. $M \pm$ SE. *Different from control, # different from same treatment without methyl-β-cyclodextrin ($p < 0.05$, ANOVA).

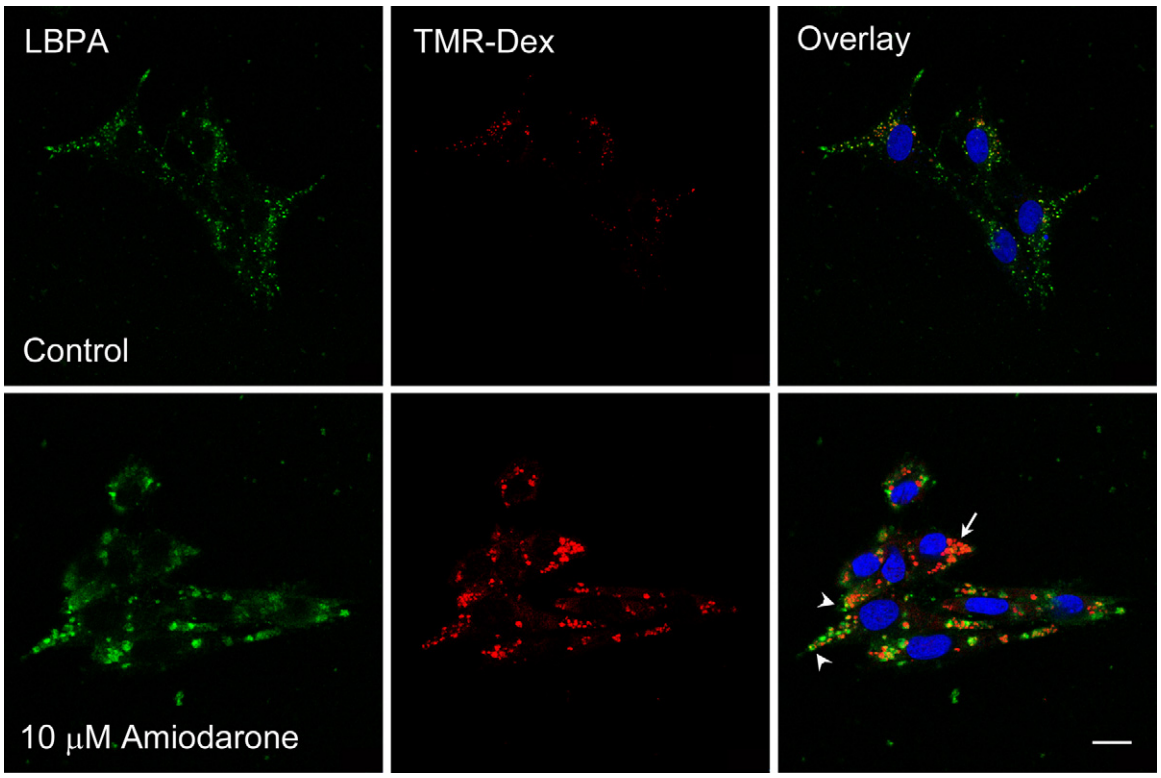


**Fig. 7.** Amiodarone alters fluid phase endocytosis. BHK cells were loaded for 12 h with tetramethylrhodamine dextran (TMR-Dex) and then were chased for 5 h either with or without 10 μM amiodarone. The distribution of TMR-Dex (red) and LBPA (green) was then analyzed by confocal microscopy. Nuclei stained blue. Arrows indicate dilated vacuoles containing TMR-Dex. Arrowheads indicate TMR-Dex and LBPA co-localization (yellow). Bar 10 μm.

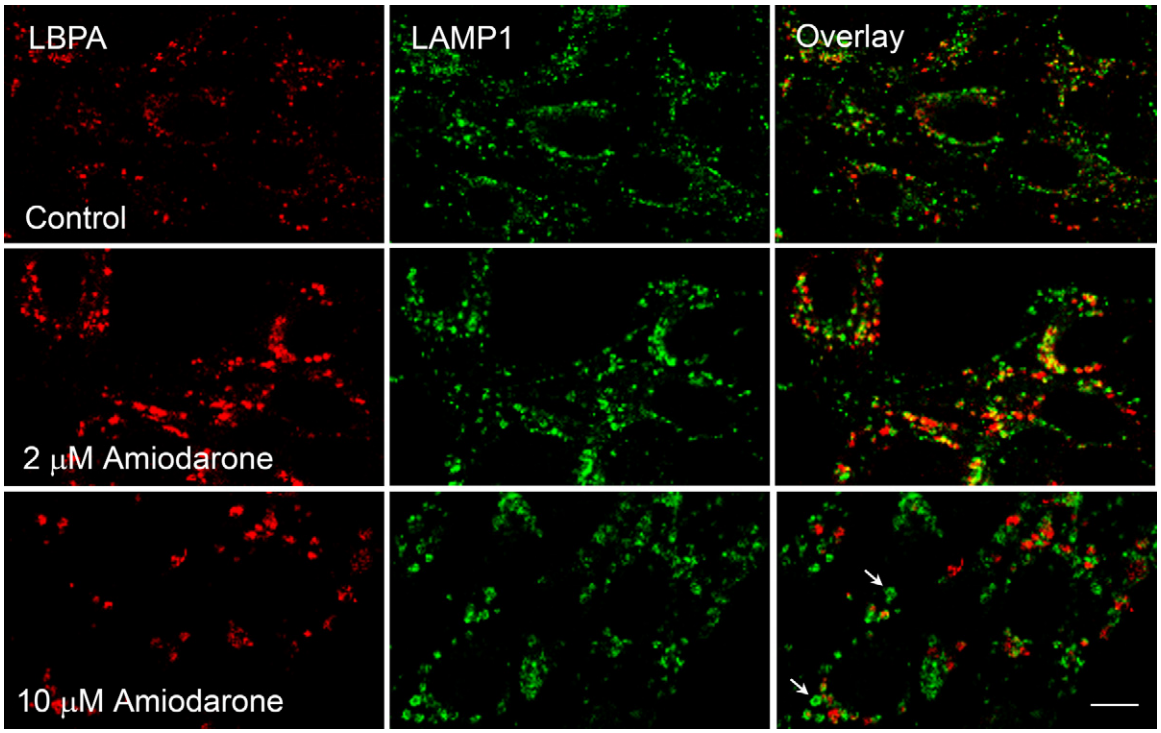


**Fig. 8.** Effect of amiodarone on the distribution of LAMP1 and LBPA. BHK cells, incubated for 16 h with 0–10 μM amiodarone, were stained with antibodies to LAMP1 and LBPA and then were analyzed with confocal microscopy. Arrows: ring-like structures containing LAMP1. Bar 10 μm.

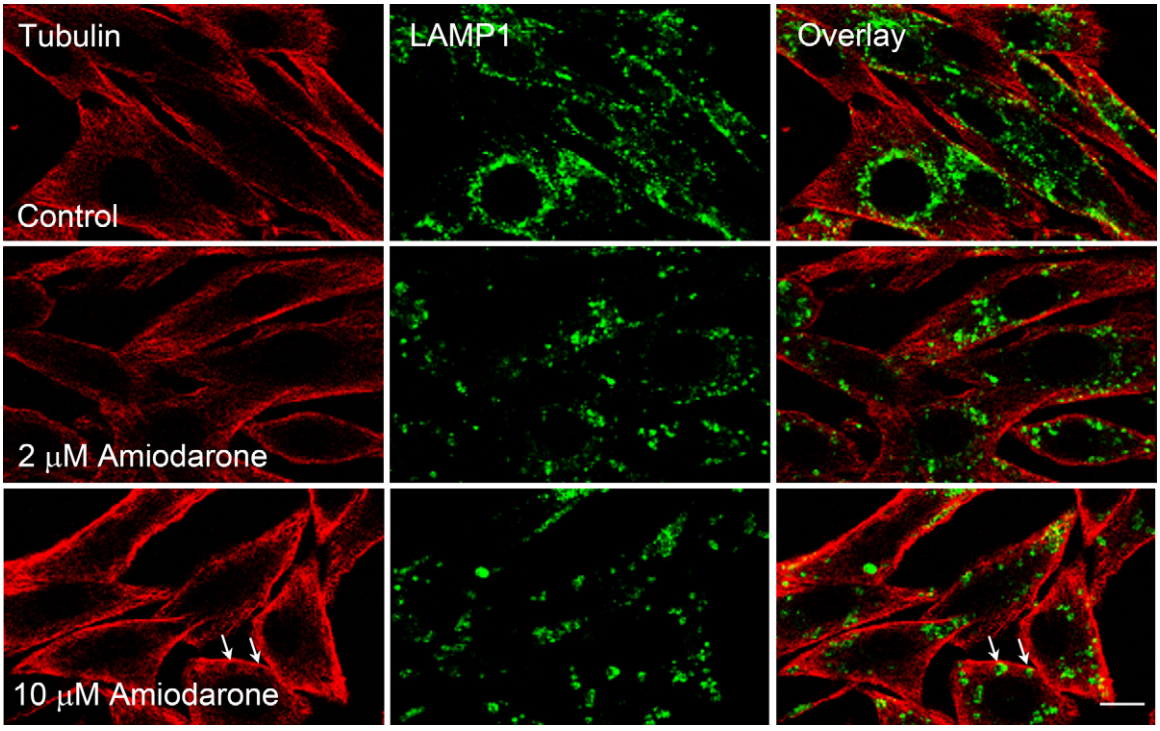


**Fig. 9.** Effect of amiodarone on the distribution of LAMP1 and tubulin. BHK cells, incubated for 16 h with 0–10 μM amiodarone, were stained with antibodies to LAMP1 and tubulin and then were analyzed with confocal microscopy. Arrows: aggregates of LAMP1 surrounded by a rim of tubulin. Bar 10 μm.

concentrated into less numerous but larger structures, as seen for LBPA. Aggregates of LAMP1 induced by amiodarone had different morphology, presenting as clumps or tiny rings (Fig. 8), as spots arranged along the rim of dilated structures (Fig. 1S) or as components of structures surrounded by a rim of tubulin (Fig. 9). Interestingly co-localization between LAMP1 and LBPA, which was moderate in control cells, increased after incubation with 2 μM amiodarone but was almost nil after incubation with 10 μM amiodarone, suggesting that low concentrations of the drug might stimulate heterotypic fusion of organelles, while high concentrations could induce homotypic fusion.

The changes in the distribution of LAMP1 induced by amiodarone agree with changes in the distribution of NPC1 protein, a multispanning protein inserted in the limiting membrane of late endosomes/lysosomes which, when mutated, is the most frequent cause of Niemann-Pick type C disease [16,47–49]. Indeed, as shown in Fig. 10, in control cells NPC1 had a point-like distribution and co-localized partially with LBPA, while in cells incubated with 10 μM amiodarone it coalesced into large aggregates spatially separated from LBPA.

To further characterize the effects of amiodarone on late endosomes we studied its effects on the secretion of exosomes,

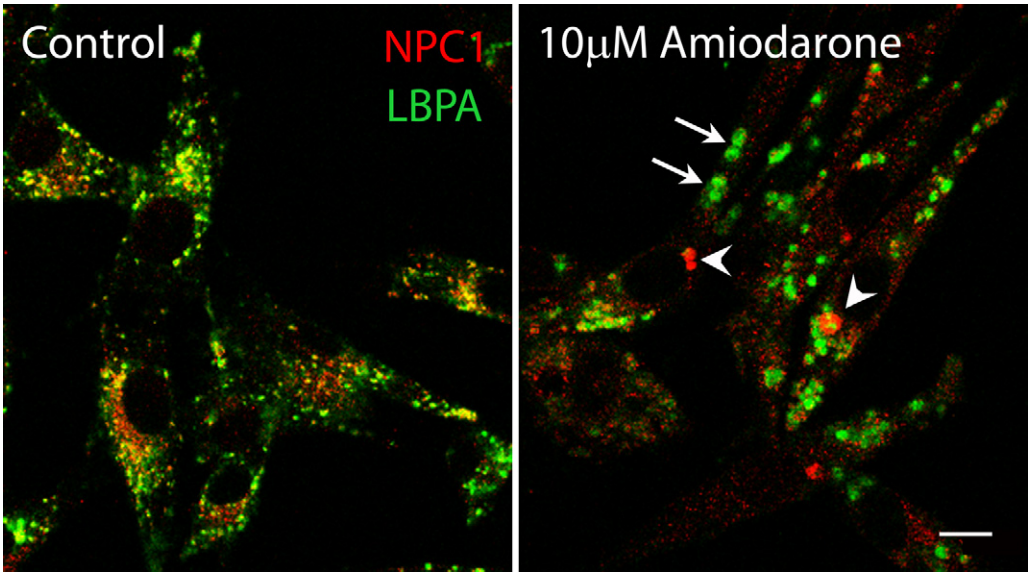


**Fig. 10.** Amiodarone induces aggregates of NPC1 protein spatially separated from aggregates of LBPA. BHK cells incubated for 16 h with 0 or 10 μM amiodarone were stained with antibodies to NPC1 and LBPA and then were analyzed with confocal microscopy. Arrowheads indicate aggregates of NPC1 (red). Arrows indicate aggregates of LBPA (green). Yellow indicates co-localization.

which are vesicles located in the lumen of late endosomes/multivesicular bodies destined to be secreted in the extracellular milieu [24]. To that end K562 cells were incubated with or without 10 μM amiodarone for 16 h, secreted exosomes were then isolated by differential centrifugation and acetylcholinesterase activity associated with them was measured. We found that amiodarone decreased secreted acetylcholinesterase by $12.0 \pm 8.7\%$ with respect to control cells ($N = 7$, change not significant), indicating that interference with exosome release is unlikely to contribute significantly to the accumulation of membranes induced by amiodarone. These findings also indicate that amiodarone does not perturb the whole population of late endosomes/lysosomes.

### 3.7. Amiodarone has no effect on transferrin recycling, Shiga toxin activity and lentivirus budding

The available evidence indicates that amiodarone does not influence the distribution of markers of early endosomes. To corroborate the lack of impact on this compartment, we studied the effects of amiodarone on early endosome-dependent activities like transferrin recycling, Shiga toxin trafficking and ESCRT-dependent lentivirus budding.

The effect on transferrin recycling was analyzed by loading human monocytes with labelled transferrin and then measuring its release in the presence of 0 or 10 μM amiodarone. As shown in Fig. 2S, amiodarone had no effect on transferrin recycling.

The effect on Shiga toxin activity was analyzed by incubating Vero cells with Shiga toxin 1 in the presence or in the absence of 0–20 μM amiodarone for a time sufficient for the toxin to be taken up, processed in early endosomes, transferred to the Golgi and then moved to the cytoplasm, where it inhibits protein synthesis [26,49]. As shown in Fig. 2S the activity of Shiga toxin was not decreased by amiodarone, suggesting a correct processing and trafficking of the toxin.

The human immunodeficiency virus type 1 (HIV-1) and other lentiviruses, such as the feline immunodeficiency virus (FIV) exit infected cells by budding from the plasma membrane, a process requiring membrane fission. The only viral component involved in budding is the structural protein Gag, which executes budding by recruiting host proteins belonging to the ESCRT complexes, such as

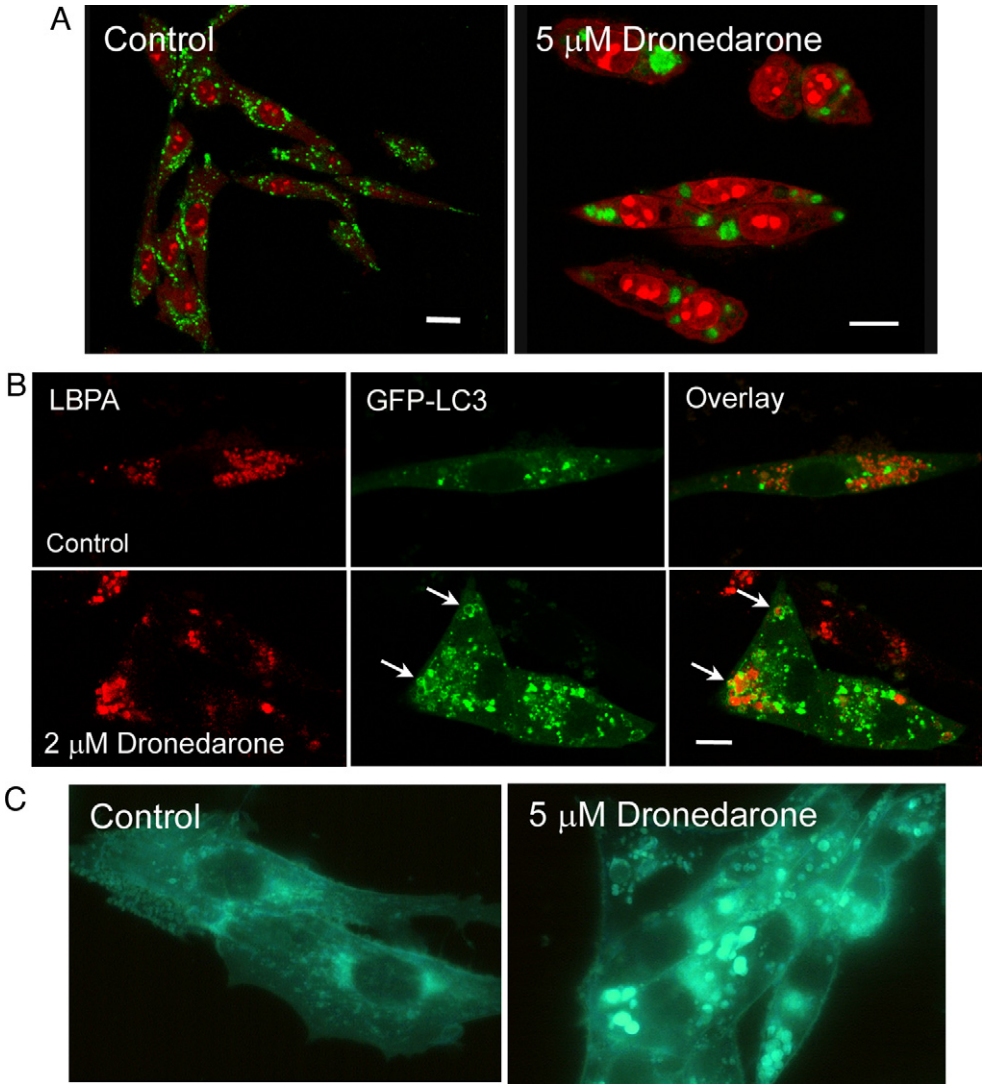


**Fig. 11.** Dronedarone alters the distribution of LBPA and unesterified cholesterol and stimulates autophagy. (A) Confocal images of BHK cells incubated for 16 h with 5 μM dronedarone, stained for LBPA (green) and then counterstained with propidium iodide (red). (B) BHK cells, transiently transfected with pEGFP-LC3 plasmid, were incubated for 16 h with control medium or with 2 μM dronedarone. The distribution of LBPA (red) and LC3 (green) was then analyzed by confocal microscopy. Arrow: LC3 positive membranes surrounding LBPA aggregates. (C) Epifluorescence image of BHK cells incubated for 16 h with 0 (control) or 5 μM dronedarone and then incubated with filipin to stain unesterified cholesterol.

Tsg101 and AIP1 [50]. To understand whether amiodarone interferes with the ESCRT complex, 293T cells were transfected with constructs expressing either the feline immunodeficiency virus (pΔenv1) or the human immunodeficiency type 1 (pSVC21) Gag/Pol. Twenty four hours post-transfection, cells were incubated with 0 or 10 μM amiodarone for additional 24 h. Virus like particles (VLP) released in the supernatant and cells were then analyzed by SDS-PAGE electrophoresis followed by Western blotting using antibodies specific for either FIV or HIV-1 capsid proteins. As shown in Fig. 2S, amiodarone did not affect synthesis and processing of the intracellular Gag protein and did not inhibit the release of mature VLPs, suggesting lack of interference with budding. Collectively these experiments support the view that amiodarone affects only late compartments of the endocytic pathway.

### 3.8. Dronedarone alters the distribution of cell lipids and stimulates autophagy

Dronedarone is a non-iodinated benzofuran derivative, recently introduced in clinical practice to get around some of amiodarone not desirable effects like slow pharmacokinetics and iodine-related thyroid damage [27]. Previous experiments with rabbit alveolar macrophages have shown that amiodarone induces the formation of vacuoles and inclusion bodies [28], but the mechanism of formation of these structures has not been studied. To clarify this, BHK cells were incubated with 0–5 μM dronedarone for 16 h (higher concentrations were toxic to cells) and then the distribution of LBPA and unesterified cholesterol were analyzed. As shown in Fig. 11 cells treated with dronedarone had severe disturbances in the distribution LBPA and unesterified cholesterol. Since dronedarone has relatively high pKa and a very high solubility in water at pH 5, the strong effect on LBPA distribution agrees with the view that these physico-chemical properties play an important role in the interference with late compartments of the endocytic pathway (Tables 1 and 2).

Since autophagy is up-regulated by amiodarone [7], we studied the effect of dronedarone on the distribution of transiently expressed eGFP-LC3, a protein present at all steps along the autophagic pathway [51]. We found that in control cells LBPA and LC3 had a point-like distribution, whereas in cells treated with 2 μM dronedarone (the highest concentrations tolerated by transfected cells) or 10 μM amiodarone, LBPA and LC3 changed from a point-like to a clump-like distribution (Fig. 11 and 3S). At some places aggregates of LBPA were enclosed by ring-like structures decorated with LC3, as expected during the formation of amphisomes, which are intermediate organelles formed during autophagy. Thus, like amiodarone, dronedarone also alters the distribution of cell lipids and induces autophagy.

## 4. Discussion

### 4.1. Vacuoles and inclusion bodies induced by amiodarone

This study shows that vacuoles and inclusion bodies forming in the presence of amiodarone originate from late compartments of the endocytic pathway, since they display markers normally associates with late endosomes/lysosomes, like Rab7, LAMP1, NPC1, LBPA. It also shows that separate populations of organelles pertaining to late endocytic compartments are affected, as indicated by the lack of co-localization of aggregates of LBPA, LAMP1 and NPC1 at high amiodarone concentrations. Finally it shows that amiodarone does not affect the whole of late endosome activities, since the secretion of exosomes does not change.

Vacuoles and inclusion bodies appear to form by several mechanisms: block of fluid phase endocytosis, inappropriate fusion of organelles, collapse of lumenal structures, accumulation of undegraded substrates and accumulation of wrongly trafficked lipids. Other mechanisms could also be at play. For example in normal cells late endosomes fuse with lysosomes, forming hybrid organelles from which lysosomes reform when the degradation of substrates is complete [52]. We posit that decreased reformation of lysosomes from hybrid intermediates could contribute to the vacuolar phenotype induced by amiodarone. Such a mechanism could explain the decreased lysosome yield detected in alveolar macrophages treated with amiodarone [9] and the finding that incubation of BHK cells for 16 h with 10 μM amiodarone does not modify the total cell content of LAMP-1, a protein inserted in the limiting membrane of lysosomes (not shown).

This study also shows that amiodarone does not directly affect early endosomes, since: (a) it does not alter the distribution of early endosome markers; (b) does not inhibit binary toxins requiring functional early endosomes for activation, like Shiga toxin 1; (c) does not disturb transferrin recycling; (d) does not interfere with the budding of lentiviruses depending upon the recruitment of a highly conserved set of proteins, dubbed the endosomal sorting complexes required for transport (ESCRTs), also required for the formation of multivesicular bodies in early endosomes [14,53]. To directly confirm the lack of interference with the ESCRTs, we studied the effect of amiodarone on the formation of lumenal vesicles by isolated early endosomes [54]. To that end the post-nuclear supernatant obtained from BHK cells cultured for 3 h in the presence of 0–20 μM amiodarone, was incubated at 37 °C with the non permeant fluorescent probe 8-hydroxypyrene-1,3,6-trisulfonic acid in the presence of an energy donor system and trapping of the probe in the interior of vesicles forming by inward budding of endosome limiting membrane was allowed to take place for 20 min. Subsequently, after quenching the extra-organellar fluorescence with p-xylene-bis-pyridinium bromide, endosomes were isolated by flotation and the fluorescence associated with them was measured. In 3 separated experiments we found no change in endosome-associated fluorescence after incubation with amiodarone. Thus several lines of evidence indicate that amiodarone has no direct effect on early endosomes. It is possible, however, that chronic exposure to the drug might reverberate on early endosomes also, perhaps by modifying the global trafficking of membranes or through the sequestration of critical lipids.

Cell changes induced by amiodarone have thus far been included under the term "phospholipidosis", a term based on electron microscopy, which describes the formation of multilaminar inclusion vesicles [1,2]. The accumulation of LBPA, cholesterol and glycosphyngolipids in cells exposed to amiodarone is compatible with the accumulation of membranes observed at the electron microscope. It appears, however, that the term phospholipidosis does not fully portray the cell changes induced by amiodarone since it does not reflect the accumulation of other lipid species besides phospholipids and does not include other effects, like disturbances in fluid phase endocytosis.

### 4.2. The target of amiodarone activity

Data obtained with amiodarone analogues (Table 2) indicate that high pKa and especially high water-solubility at acidic pH are important determinants of the interference of amiodarone with late endosomes/lysosomes. Since basic pKa and low membrane permeability, favour the sequestration of weakly basic amines in the lumen of acidic organelles [55], we infer that amiodarone target resides into or is accessible from the lumen of late endosomes/lysosomes. The nature of amiodarone target remains to be clarified since the present results are compatible

both with the inhibition of specific component(s) accessible from the luminal side and with an aspecific effect, like the competition of amiodarone with polycationic lipid hydrolases or activator proteins for the negative surface of late endosome/lysosome internal membranes [56]. The last mechanism, recently proposed for other cationic amphiphilic drugs, would explain the accumulation of different classes of undegraded lipids and the membrane traffic jam within late endosomes/lysosomes [57].

The propensity to be trapped in the lumen of acidic organelles could also explain the preferential effect of amiodarone on late endosomes/lysosomes, whose interior is more acidic than that of early endosomes. On the other side it remains at present unclear how amiodarone may target specific sets of organelles pertaining to late endosomes/lysosomes.

### 4.3. Amiodarone induces a phenotype reminiscent of Niemann-Pick type C disease

The phenotype induced by amiodarone recalls Niemann-Pick type C disease, a complex lysosomal storage disorder characterized by the accumulation of different sorts of lipids in late endosomes/lysosomes, by defective lysosomal calcium homeostasis and unique trafficking defects [20]. NPC disease is caused by mutations in the NPC1 or NPC2 genes, which encode respectively NPC1, a multispanning trans-membrane domain protein located on the limiting membrane of late endosomes/lysosomes and NPC2, a soluble lysosomal protein [58].

There are differences, however, between changes induced by amiodarone and the NPC phenotype. In fact on one side methyl-β-cyclodextrin worsens the effects of amiodarone on the distribution of LBPA, while, on the contrary, it alleviates the redistribution of LBPA caused by U18666A. On the other side budding of HIV-1 virus is inhibited in NPC cells or by treatment with U18666A [58], but is not affected by amiodarone. Thus, rather than recapitulating the whole pathogenetic cascade of NPC disease, changes induced by amiodarone might exemplify a common theme observed when damage to late endosomes/lysosomes disturbs pathways intersecting at this crucial spot. As an example, cells lacking prosaposin, a protein cofactor necessary for glycosphingolipid degradation, present enlarged electron-lucent structures of late endosomal origin, accumulate unesterified cholesterol and display altered trafficking of BODIPY-LacCer [59].

### 4.4. Clinical implications

Atrial fibrillation predisposes patients to stroke, heart failure and death and affects nearly 1 every 10 persons aged 80 years and older [60]. Among conventional antiarrhythmic drugs amiodarone has proved by far the most effective at maintaining sinus rhythm, but effectiveness is diminished by long elimination half-life, iodine-induced thyroid toxicity and acute lung damage. In an attempt to relieve some of these problems, dronedarone, a non-iodinated benzofuran derivative, has been recently introduced in clinical practice [27]. Dronedarone has multichannel blocking properties comparable to those of amiodarone but is more potent at blocking peak sodium currents and acetylcholine activated potassium currents and has stronger antiadrenergic effects [27]. On the basis of the present evidence it appears that, on a molar basis, dronedarone is at least as potent as amiodarone with respect to interference with late compartments of the endocytic pathway. Dronedarone, however, is metabolized rapidly and reaches serum levels over 10 times lower than in patients treated with amiodarone [27], thus the clinical relevance of its interference with late endocytic compartments remains to be determined.

### 4.5. Future directions

The interference of amiodarone and its derivatives with the endocytic pathway, besides its obvious clinical interest in the field of cardiology, might represent the subject of future investigations in unrelated areas, in particular for the development of novel strategies against infectious agents. Indeed amiodarone interferes *in vitro* with the life cycle of the SARS coronavirus [6], mitigates in an *in vivo* model the effects of the encephalomyocarditis virus [61] and has been shown to be of value in the treatment of the Trypanosomacruzi infection [62]. In addition, it could be of interest studying the effect of amiodarone on Dengue infection, because it has recently been shown that LBPA (whose distribution may be modified by amiodarone) is an obligatory cofactor for the entry of the Dengue virus into target cells [63].

### 4.6. Conclusion

Amiodarone induces the formation of vacuoles and inclusion bodies by interfering with late compartments of the endocytic pathway. Mechanisms of formation of vacuoles and inclusion bodies include disturbances in the progression of fluid phase endocytosis, inappropriate fusion of organelles, collapse of lumenal structures, accumulation of undegraded substrates and accumulation of wrongly trafficking lipids. High water-solubility at acidic pH is a crucial requirement for the interference of amiodarone with late endosomes/lysosomes. Dronedarone is at least as potent as amiodarone with respect to interference with late compartments of the endocytic pathway. The interference of amiodarone with late endosomes/lysosomes may be of value in areas outside the field of arrhythmology.

## Acknowledgements

We thank Prof. E. Papini and Dr F. Tonello, University of Padova, Italy, Prof. C. Bucci, University of Lecce, Italy and Dr J.P. Krise, University of Kansas, KA, for help and advice. We also thank Prof. M. Brigotti, University of Bologna, Italy, for preparing Shiga toxin 1. This work was supported in part by Progetti di Ateneo, University of Padova, 2008 to A.B.

## Appendix A. Supplementary data

Supplementary data associated with this article can be found, in the online version, at doi:10.1016/j.bcp.2011.07.090.

## References

[1] Vassallo P, Trohman RG. Prescribing amiodarone: an evidence-based review of clinical indications. J Am Med Assoc 2007;298:1312–22.
[2] Zimetbaum P. Amiodarone for atrial fibrillation. N Engl J Med 2007;356:935–41.
[3] Pollak PT, Bouillon T, Shafer SL. Population pharmacokinetics of long-term oral amiodarone therapy. Clin Pharmacol Ther 2000;67:642–52.
[4] Adams PC, Holt DW, Storey GC, Morley AR, Callaghan J, Campbell RW. Amiodarone and its desethyl metabolite: tissue distribution and morphologic changes during long-term therapy. Circulation 1985;72:1064–75.
[5] Brien JF, Jimmo S, Brennan FJ, Ford SE, Armstrong PW. Distribution of amiodarone and its metabolite, desethylamiodarone, in human tissues. Can J Physiol Pharmacol 1987;65:360–4.
[6] Stadler K, Ha HR, Ciminale V, Spirli C, Saletti G, Schiavon M, et al. Amiodarone alters late endosomes and inhibits SARS coronavirus infection at a post-endosomal level. Am J Respir Cell Mol Biol 2008;39:142–9.
[7] Morissette G, Ammoury A, Rusu D, Marguery MC, Lodge R, Poubelle PE, et al. Intracellular sequestration of amiodarone: role of vacuolar ATPase and macroautophagic transition of the resulting vacuolar cytopathology. Br J Pharmacol 2009;157:1531–40.
[8] Ha HR, Bigler L, Wendt B, Maggiorini M, Follath F. Identification and quantitation of novel metabolites of amiodarone in plasma of treated patients. Eur J Pharm Sci 2005;24:271–9.

[9] Baritussio A, Marzini S, Agostini M, Alberti A, Cimenti C, Bruttomesso D, et al. Amiodarone inhibits lung degradation of SP-A and perturbs the distribution of lysosomal enzymes. Am J Physiol Lung Cell Mol Physiol 2001;281:L1189–9.
[10] Sanchez AM, Thomas D, Gillespie EJ, Damoiseaux R, Rogers J, Saxe JP, et al. Amiodarone and bepridil inhibit anthrax toxin entry into host cells. Antimicrob Agents Chemother 2007;51:2403–11.
[11] Mortuza GB, Neville WA, Delaney J, Waterfield CJ, Camilleri P. Characterisation of a potential biomarker of phospholipidosis from amiodarone-treated rats. Biochim Biophys Acta 2003;1631:136–46.
[12] Kobayashi T, Beuchat MH, Lindsay M, Frias S, Palmiter RD, Sakuraba H, et al. Late endosomal membranes rich in lysobisphosphatidic acid regulate cholesterol transport. Nat Cell Biol 1999;1:113–8.
[13] Puhar A, Montecucco C. Where and how do anthrax toxins exit endosomes to intoxicate host cells? Trends Microbiol 2007;15:477–82.
[14] Raiborg C, Stenmark H. The ESCRT machinery in endosomal sorting of ubiquitylated membrane proteins. Nature 2009;458:445–52.
[15] Chevallier J, Chamoun Z, Jiang G, Prestwich G, Sakai N, Matile S, et al. Lysobisphosphatidic acid controls endosomal cholesterol levels. J Biol Chem 2008;283:27871–80.
[16] Brown MS, Goldstein JL. A receptor-mediated pathway for cholesterol homeostasis. Science 1986;232:34–47.
[17] Xie C, Turley SD, Pentchev PG, Dietschy JM. Cholesterol balance and metabolism in mice with loss of function of Niemann-Pick C protein. Am J Physiol 1999;276:E336–44.
[18] Goldman SD, Krise JP. Niemann-Pick C1 functions independently of Niemann-Pick C2 in the initial stage of retrograde transport of membrane-impermeable lysosomal cargo. J Biol Chem 2010;285:4983–94.
[19] Liscum L, Ruggiero RM, Faust JR. The intracellular transport of low density lipoprotein-derived cholesterol is defective in Niemann-Pick type C fibroblasts. J Cell Biol 1989;108:1625–36.
[20] Lloyd-Evans E, Platt FM. Lipids on trial: the search for the offending metabolite in Niemann-Pick type C disease. Traffic 2010;11:419–28.
[21] Liu B, Turley SD, Burns DK, Miller AM, Repa JJ, Dietschy JM. Reversal of defective lysosomal transport in NPC disease ameliorates liver dysfunction and neurodegeneration in the npc1−/− mouse. Proc Natl Acad Sci USA 2009;106:2377–82.
[22] Lachmann RH, te Vruchte D, Lloyd-Evans E, Reinkensmeier G, Sillence DJ, Fernandez-Guillen L, et al. Treatment with miglustat reverses the lipid-trafficking defect in Niemann-Pick disease type C. Neurobiol Dis 2004;16:654–8.
[23] Devlin C, Pipalia NH, Liao X, Schuchman EH, Maxfield FR, Tabas I. Improvement in lipid and protein trafficking in Niemann-Pick C1 cells by correction of a secondary enzyme defect. Traffic 2010;11:601–15.
[24] Strauss K, Goebel C, Runz H, Mobius W, Weiss S, Feussner I, et al. Exosome secretion ameliorates lysosomal storage of cholesterol in Niemann-Pick type C disease. J Biol Chem 2010;285:26279–88.
[25] Simons M, Raposo G. Exosomes—vesicular carriers for intercellular communication. Curr Opin Cell Biol 2009;21:575–81.
[26] Warnier M, Romer W, Geelen J, Lesieur J, Amessou M, van den Heuvel L, et al. Trafficking of Shiga toxin/Shiga-like toxin-1 in human glomerular microvascular endothelial cells and human mesangial cells. Kidney Int 2006;70:2085–91.
[27] Patel C, Yan GX, Kowey PR. Dronedarone. Circulation 2009;120:636–44.
[28] Quaglino D, Ha HR, Duner E, Bruttomesso D, Bigler L, Follath F, et al. Effects of metabolites and analogs of amiodarone on alveolar macrophages: structure–activity relationship. Am J Physiol Lung Cell Mol Physiol 2004;287:L438–47.
[29] Calistri A, Del Vecchio C, Salata C, Celestino M, Celegato M, Gottlinger H, et al. Role of the feline immunodeficiency virus L-domain in the presence or absence of Gag processing: involvement of ubiquitin and Nedd4-2s ligase in viral egress. J Cell Physiol 2009;218:175–82.
[30] Ratner L, Haseltine W, Patarca R, Livak KJ, Starcich B, Josephs SF, et al. Complete nucleotide sequence of the AIDS virus, HTLV-III. Nature 1985;313:277–84.
[31] Bigler L, Spirli C, Fiorotto R, Pettenazzo A, Duner E, Baritussio A, et al. Synthesis and cytotoxicity properties of amiodarone analogues. Eur J Med Chem 2007;42:861–7.
[32] Ishitsuka R, Sato SB, Kobayashi T. Imaging lipid rafts. J Biochem 2005;137:249–54.
[33] Yamaji A, Sekizawa Y, Emoto K, Sakuraba H, Inoue K, Kobayashi H, et al. Lysenin, a novel sphingomyelin-specific binding protein. J Biol Chem 1998;273:5300–6.
[34] Martin OC, Pagano RE. Internalization and sorting of a fluorescent analogue of glucosylceramide to the Golgi apparatus of human skin fibroblasts: utilization of endocytic and nonendocytic transport mechanisms. J Cell Biol 1994;125:769–81.
[35] Miedel MT, Rbaibi Y, Guerriero CJ, Colletti G, Weixel KM, Weisz OA, et al. Membrane traffic and turnover in TRP-ML1-deficient cells: a revised model for mucolipidosis type IV pathogenesis. J Exp Med 2008;205:1477–90.
[36] Baritussio A, Alberti A, Armanini D, Meloni F, Bruttomesso D. Different pathways of degradation of SP-A and saturated phosphatidylcholine by alveolar macrophages. Am J Physiol Lung Cell Mol Physiol 2000;279:L91–9.
[37] Tanner LI, Lienhard GE. Insulin elicits a redistribution of transferrin receptors in 3T3-L1 adipocytes through an increase in the rate constant for receptor externalization. J Biol Chem 1987;262:8975–80.
[38] Fader CM, Sanchez D, Furlan M, Colombo MI. Induction of autophagy promotes fusion of multivesicular bodies with autophagic vacuoles in k562 cells. Traffic 2008;9:230–50.
[39] Wright JR. Immunoregulatory functions of surfactant proteins. Nat Rev Immunol 2005;5:58–68.
[40] Duvvuri M, Konkar S, Funk RS, Krise JM, Krise JP. A chemical strategy to manipulate the intracellular localization of drugs in resistant cancer cells. Biochemistry 2005;44:15743–9.
[41] Lloyd-Evans E, Morgan AJ, He X, Smith DA, Elliot-Smith E, Sillence DJ, et al. Niemann-Pick disease type C1 is a sphingosine storage disease that causes deregulation of lysosomal calcium. Nat Med 2008;14:1247–55.
[42] Liu B, Li H, Repa JJ, Turley SD, Dietschy JM. Genetic variations and treatments that affect the lifespan of the NPC1 mouse. J Lipid Res 2008;49:663–9.
[43] Vanier MT. Lipid changes in Niemann-Pick disease type C brain: personal experience and review of the literature. Neurochem Res 1999;24:481–9.
[44] Castanho MA, Coutinho A, Prieto MJ. Absorption and fluorescence spectra of polyene antibiotics in the presence of cholesterol. J Biol Chem 1992;267:204–9.
[45] Abi-Mosleh L, Infante RE, Radhakrishnan A, Goldstein JL, Brown MS. Cyclodextrin overcomes deficient lysosome-to-endoplasmic reticulum transport of cholesterol in Niemann-Pick type C cells. Proc Natl Acad Sci USA 2009;106:19316–21.
[46] Rosenbaum AI, Zhang G, Warren JD, Maxfield FR. Endocytosis of beta-cyclodextrins is responsible for cholesterol reduction in Niemann-Pick type C mutant cells. Proc Natl Acad Sci USA 2010;107:5477–82.
[47] Infante RE, Abi-Mosleh L, Radhakrishnan A, Dale JD, Brown MS, Goldstein JL. Purified NPC1 protein. I. Binding of cholesterol and oxysterols to a 1278-amino acid membrane protein. J Biol Chem 2008;283:1052–63.
[48] Infante RE, Radhakrishnan A, Abi-Mosleh L, Kinch LN, Wang ML, Grishin NV, et al. Purified NPC1 protein: II. Localization of sterol binding to a 240-amino acid soluble luminal loop. J Biol Chem 2008;283:1064–75.
[49] Johannes L, Romer W. Shiga toxins—from cell biology to biomedical applications. Nat Rev Microbiol 2010;8:105–16.
[50] Strack B, Calistri A, Craig S, Popova E, Gottlinger HG. AIP1/ALIX is a binding partner for HIV-1 p6 and EIAV p9 functioning in virus budding. Cell 2003;114:689–99.
[51] Yang Z, Klionsky DJ. Eaten alive: a history of macroautophagy. Nat Cell Biol 2010;12:814–22.
[52] Luzio JP, Pryor PR, Bright NA. Lysosomes: fusion and function. Nat Rev Mol Cell Biol 2007;8:622–32.
[53] Hurley JH, Hanson PI. Membrane budding and scission by the ESCRT machinery: it's all in the neck. Nat Rev Mol Cell Biol 2010;11:556–66.
[54] Falguieres T, Luyet PP, Bissig C, Scott CC, Velluz MC, Gruenberg J. In vitro budding of intralumenal vesicles into late endosomes is regulated by Alix and Tsg101. Mol Biol Cell 2008;19:4942–55.
[55] Kaufmann AM, Krise JP. Niemann-Pick C1 functions in regulating lysosomal amine content. J Biol Chem 2008;283:24584–93.
[56] Wilkening G, Linke T, Uhlhorn-Dierks G, Sandhoff K. Degradation of membrane-bound ganglioside GM1. Stimulation by bis(monoacylglycero)phosphate and the activator proteins SAP-B and GM2-AP. J Biol Chem 2000;275:35814–9.
[57] Wilkening G, Linke T, Sandhoff K. Lysosomal degradation on vesicular membrane surfaces. Enhanced glucosylceramide degradation by lysosomal anionic lipids and activators. J Biol Chem 1998;273:30271–8.
[58] Tang Y, Leao IC, Coleman EM, Broughton RS, Hildreth JE. Deficiency of Niemann-Pick type C-1 protein impairs release of human immunodeficiency virus type 1 and results in Gag accumulation in late endosomal/lysosomal compartments. J Virol 2009;83:7982–95.
[59] Kiss RS, Ma Z, Nakada-Tsukui K, Brugnera E, Vassiliou G, McBride HM, et al. The lipoprotein receptor-related protein-1 (LRP) adapter protein GULP mediates trafficking of the LRP ligand prosaposin, leading to sphingolipid and free cholesterol accumulation in late endosomes and impaired efflux. J Biol Chem 2006;281:12081–92.
[60] Furberg CD, Psaty BM, Manolio TA, Gardin JM, Smith VE, Rautaharju PM. Prevalence of atrial fibrillation in elderly subjects (the Cardiovascular Health Study). Am J Cardiol 1994;74:236–41.
[61] Ito H, Ono K, Nishio R, Sasayama S, Matsumori A. Amiodarone inhibits interleukin 6 production and attenuates myocardial injury induced by viral myocarditis in mice. Cytokine 2002;17:197–202.
[62] Adesse D, Azzam EM, Meirelles Mde N, Urbina JA, Garzoni LR. Amiodarone inhibits Trypanosoma cruzi infection and promotes cardiac cell recovery with gap junction and cytoskeleton reassembly in vitro. Antimicrob Agents Chemother 2011;55:203–10.
[63] Zaitseva E, Yang ST, Melikov K, Pourmal S, Chernomordik LV. Dengue virus ensures its fusion in late endosomes using compartment-specific lipids. PLoS Pathog 2010;6.